Doctoral Thesis

Catalysts design in metal-oxide sensors for selective gas detection and high resistance to poisons

Yeong Min Kwon

Department of Materials Science and Engineering

Ulsan National Institute of Science and Technology

2021

Catalysts design in metal-oxide sensors for selective gas detection and high resistance to poisons

Yeong Min Kwon

Department of Materials Science and Engineering

Ulsan National Institute of Science and Technology

ULSAN NATIONAL INSTITUTE OF
SCIENCE AND TECHNOLOGY

Catalysts design in metal-oxide sensors for selective gas detection and high resistance to poisons

A thesis/dissertation submitted to
Ulsan National Institute of Science and Technology
in partial fulfillment of the
requirements for the degree of
Doctor of Philosophy

Yeong Min Kwon

06.15.2021 of submission
Approved by

Advisor
Kyoung Jin Choi

Catalysts design in metal-oxide sensors for selective gas detection and high resistance to poisons

Yeong Min Kwon

This certifies that the thesis/dissertation of Yeong Min Kwon is approved.

06.15.2021 of submission

Signature

Advisor: Kyoung Jin Choi

Signature

Seungho Cho

Signature

Heungjoo Shin

Signature

Jae Joon Kim

Signature

Jeong Min Baik

*three signatures total in case of masters

Abstract

Advances in technology are replacing the things that humans had to do or becoming human hands and feet. In the future, the life of robots mixing with humans is not something that can only be seen in science fiction movies but is getting closer to reality. For the development of these future technologies or robots, the development of sensor technology is indispensable. The composition and function of the sensor have something in common with humans, and just like humans accept and respond to any stimulus, the sensor also has such a reaction system. The sensor consists of a receptor that inputs a response and a transducer that converts various external reactions into electrical signals and can output a response with an actuator that outputs these electrical signals as a reaction. If human skin or various senses are receptors for sensors, transducers can be seen as neurons that transmit the stimuli of the senses that humans responded to. In addition, it can be interpreted as an actuator that is judged by the brain and responds to stimuli through the nervous system again through neurons. A device that converts physical and chemical energy signals into electrical signals and outputs a result can be called a sensor.

In addition, many scientists and researchers have recently been interested in gas sensors for harmful gas detection, as the public is concerned about the increase in industrial accidents caused by dangerous or explosive gases that are difficult to detect with human smell. In this study, metal oxide semiconductor nanostructures were synthesized, catalysts and additives were added to make sensing materials, and they were applied to gas sensors. First, a highly selective gas detection strategy is described based on the continuous iteration method of various kinds of nanowires (WO_3, TiO_2, SnO_2, CuO, and ZnO) growth at single wafer level and the catalytic function of silver nanoparticles. The catalytic process occurring on the silver and the nanowires depended on the magnitude of barrier height at the interface which determined the electron exchange rate across the interface when it was exposed to gases, resulted in different gas responses among the nanowires. The sensor array with palladium and silver nanoparticles was tested for the ability to distinguish between the hydrogen, carbon monoxide, and nitric dioxide with detection limits ranging from sub-ppm to ppm levels, enabled the gas responses to be separated into three classes using linear discriminant analysis. Second, A stable hydrogen detection strategy based on the highly dispersive cerium oxide (CeO_2) nanoparticles/porous reduced graphene oxides (rGO) coated onto ZnO nanowires in air/Hexamethyldisiloxane (HMDSO) environment at 250°C is described. The response ($R_a/R_g = 5.88$) of palladium decorated ZnO sensor is deteriorated by the decrease of hydroxyl groups and the increase of oxygen vacancies occurring at the surface by the HMDSO. The chemical processes are strongly influenced by the oxygen supply by the CeO_2 and the SiO_2 layer is also thinner by the rGO layer. These make the sensor less sensitive to HMDSO exposure, demonstrating excellent long-term stability. Through the above research, we were able to have the technology for nanoparticle growth and understand the change in sensor characteristics according to the

catalyst addition. In addition, by developing a technology for maintaining the performance of the sensor for a long time, the sensor can be used stably for a longer time.

Contents

LIST OF FIGURES

CHAPTER 1. INTRODUCTION

A sensor refers to a device that converts non-electrical signals such as physical or chemical signals into electrical signals such as resistance, voltage, and current. The gas sensor also refers to an element that converts the reaction result of the gas molecule formed by receiving an external chemical signal and the sensor into an easy-to-measure electrical signal. There are many kinds of dangerous gases around us. Currently, environmental pollution is a serious social problem, and human sensory organs cannot determine many of these dangerous gases or quantify gas concentrations, so gas sensors, which are gas sensors that can determine gas types or concentrations, are needed. The general conditions for the gas sensor to be equipped are (1) good selectivity to react only to the gas to be detected and not be affected by other gases, and (2) high sensitivity to obtain a sufficient signal for the gas to be detected. (3) It must have a fast response speed and be able to repeat measurements. (4) It must have stability so that it can show a stable sensitivity without being affected by ambient temperature and humidity.

Gas sensors can be largely classified into semiconductor type, catalytic combustion type, electrochemical type, and optical type according to the detection method of the target gas.

A semiconductor gas sensor refers to a sensor that uses a change in electrical conductivity when a target gas meets a ceramic semiconductor surface. In oxide semiconductors among ceramic semiconductors, when a target gas is adsorbed on the oxide semiconductor surface, the thickness of the depletion layer on the surface changes due to the movement of electrons, and this change causes a change in the electrical conductivity of the semiconductor. Metal oxides, which are stable at high temperatures, are mainly used as sensing materials because high temperatures are required to shorten the sensing time, and SnO_2 is the most representative among them. The semiconductor type gas sensor reacts to most harmful gases or combustible gases and has the advantage that it is easy to manufacture as a sensor and can be mass-produced because the configuration of the detection circuit is simple, but the electrical conductivity changes even by gases other than the target gas. There is also a disadvantage of poor selectivity.

The catalytic combustion gas sensor refers to a sensor that detects the presence and concentration of gas by converting the heat of reaction between oxygen and combustible gas into an electric signal. The catalytic combustion gas sensor operates by using a combustion reaction that occurs when the target gas meets the heated carrier after heating the carrier by embedding a metal heating wire in a porous ceramic. In the case of metal, the resistance value increases as the temperature increases. As it increases, the concentration of gas is detected using the change in the resistance value of the metal due to the reaction heat generated during the contact combustion reaction. Since it is stable against humidity or temperature changes, it is mainly used for flammable gas alarms, but it has a disadvantage that it is difficult to detect high-concentration gas.

An electrochemical gas sensor refers to a sensor that detects changes in current values caused by oxidation and reduction reactions between anode and cathode in an electrolyte. Electrochemical gas sensors consist of sensing electrodes that undergo oxidation reactions, counter-electrodes that simultaneously occur reduction reactions, and reference electrodes that detect changing potentials and maintain constant potentials with oxidation and reduction reactions. Depending on the operating principle, it is divided into a galvanic cell method and a static electrolytic method, and has the advantage of excellent selectivity, stability, reactivity, and reproducibility.

Optical gas sensors measure the light absorption of gas molecules and convert them into concentrations, and typically have a non-dispersive infrared method. The non-dispersive infrared method refers to a method of measuring gas concentration from reduction of an electric signal according to the degree of infrared light absorption in a target gas using an infrared filter existing between an infrared light source and an infrared sensor. The optical gas sensor has advantages such as low power consumption, high measurement precision, and fast reaction time compared to the electrochemical formula, and is mainly used for CO_2 gas measurement.

Among gas sensors, semiconductor sensors are very interested in semiconductor sensors because semiconductor sensors have the advantage of increasing selectivity for certain gases by using economical and appropriate additives due to their sensitivity, fast detection, and low price compared to other materials. In addition, semiconductor devices have advantages in that they have high potential for diversity in form, miniaturization, weight reduction and high performance, and easy signal processing [1]. In order to improve the characteristics of oxide semiconductor gas sensor devices, fundamental considerations on physical properties, surface adsorption and desorption properties, or electrical signal changes have been the subject of major research. However, despite these efforts, there are still unresolved problems in selectivity, reproducibility, and reliability, so that high performance and application fields are limited, and excessive power consumption when applied to a portable device is exposed as a problem.

It is known by many researchers that controlling the catalytic action of gas-sensing materials is one of the most effective ways to improve gas-sensing performance [2]. This catalytic action refers to a reaction in which the catalyst replaces the detection material on the surface of the gas detection material or directly participates in the reaction when detecting the target gas. Noble metals such as platinum [3], palladium [4], silver [5], and copper [6] are highly efficient catalysts and play a role in accelerating the reaction to the target gas on the surface of the gas sensing layer.

In the work described herein, we synthesize various kinds of metal oxides (TiO_2, CuO, ZnO, SnO_2, WO_3) into various forms (nanorods, nanowires, nanoparticles) and then fabricated with gas sensors to evaluate their properties. In addition, a study was conducted to improve the characteristics of the sensor by adding catalysts (Pd, Ag) and to prevent the change of the sensor characteristics by external factors.

CHAPTER 2. THEORICAL BACKGROUND OF METAL OXIDE SEMICONDUCTOR GAS SENSOR

2.1 Basic principle of metal oxide semiconductor gas sensor

In pure oxide semiconductors, semiconductors are often made by non-stoichiometric composition changes of crystals. That is, in the case of semiconductorization due to a relative deficiency or excess of metal ions or oxygen ions in metal oxides, such lattice defects act as donors or acceptors. Materials commonly used as gas sensors such as SnO_2, ZnO, In_2O_3, etc. are n-type semiconductors in which metal ions exist in excess compared to oxygen ions. The surface level of a semiconductor is due to the surface characteristics when crystals are cut, and the adsorption of gases on the surface of a semiconductor can be divided into physical adsorption and chemical adsorption. When gas is chemically adsorbed on the surface of a semiconductor, if the electron affinity of the adsorbed species is greater than the work function of the semiconductor, negative charges are adsorbed, and if the ionization energy of the adsorbed species is less than the work function of the semiconductor, positive charges are adsorbed to form an electric double layer [7]. For example, oxygen adsorbs negative charges and hydrogen adsorbs positive charges. As shown in Fig. 1, since the surface electrical conductivity of the semiconductor changes according to the concentration of the semiconductor surface and the internal main current carrier (electrons and holes), it is predicted that the electrical conductivity of the porous sintered body with a large adsorption surface area is larger due to adsorption than that of the single crystal. Looking at the potential characteristics at the interface, when the oxide semiconductor is heated to a high temperature, the adsorption species is activated, oxygen in the air receives electrons from the device and adsorbs negative charges on the surface, and a depletion layer is formed on the surface of the semiconductor. As the negative charge adsorption of oxygen increases, the band bending of the depletion layer becomes severe as shown in Fig. 1, and the negative charge adsorption is limited.

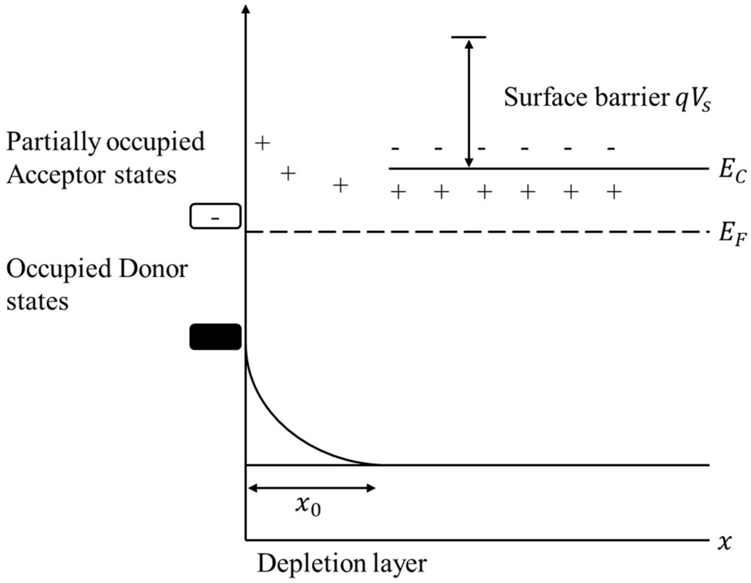

Figure 3. Schematic diagram of n-type oxide semiconductor with negatively charged surface.

Since gas sensors generally operate in air, oxygen adsorbing species are present on the surface. Since these adsorbed species receive electrons from the semiconductor and adsorb negative charges, a depletion layer is formed on the semiconductor surface. For current to flow into the device, the conductivity of the grain boundary is inversely proportional to the exponential function of the surface electric potential barrier because it must cross the surface potential barrier of the grain boundary formed by the depletion layer of each particle. In this state, when the reducing gas reacts with the adsorbed oxygen, electrons return to the device, so that the height of the barrier decreases and the resistance decreases.

This process is formulated as follows. In Figure 1, the amount of charge on adsorbed oxygen is equal to the total amount of charge in the depletion layer x_0,

$$N_s = N_D x_0 \tag{1}$$

where N_s is charge density on the surface, N_D is the donor density in the device. Solving the 1-dimensional Poisson equation as below:

$$\frac{d^2V}{dx^2} = -\frac{qN_D}{\varepsilon\varepsilon_0} \tag{2}$$

where V is potential, ε is the dielectric constant of the depletion layer, ε_0 is the dielectric constant in vacuum, integrating with $\frac{dV}{dx} = 0$ at $x = x_0$,

$$\frac{dV}{dx} = -\frac{qN_D}{\varepsilon\varepsilon_0}(x - x_0) = \frac{qN_D}{\varepsilon\varepsilon_0}(x_0 - x) \tag{3}$$

expressed as, and using the boundary condition of $V = 0$ at $x = x_0$,

$$V = -\frac{qN_D}{2\varepsilon\varepsilon_0}(x_0 - x)^2 \tag{4}$$

at surface $(x = 0)$ is same as below:

$$V_s = -\frac{qN_D{x_0}^2}{2\varepsilon\varepsilon_0} \tag{5}$$

Therefore, the carrier density at the surface is denoted as below:

$$n_s = N_D e^{-\frac{qV_S}{kT}} \tag{6}$$

The above equation is a model in which the conductivity of the device is determined by the intergranular conductivity. In this case, the overall conductivity and resistance at temperature T are expressed as below:

$$G = G_0 e^{-\frac{qV_S}{kT}} \tag{7}$$

$$R = R_0 e^{\frac{qV_S}{kT}} \tag{8}$$

If the resistance ratio before and after the reaction is defined as sensitivity when the element resistance changes according to the reaction with gas, the sensitivity S by the grain boundary model is expressed as below:

$$S = \frac{R_{air}}{R_{gas}} = e^{\frac{q\Delta V_S}{kT}} \tag{9}$$

where, R_{air} is the intergranular resistance in air, R_{gas} is intergranular resistance in gas, ΔV_s is the difference in the potential barrier according to the atmosphere change. This is the principle of operation of oxide semiconductor by grain boundary model, and Fig. 2 shows a model diagram for this.

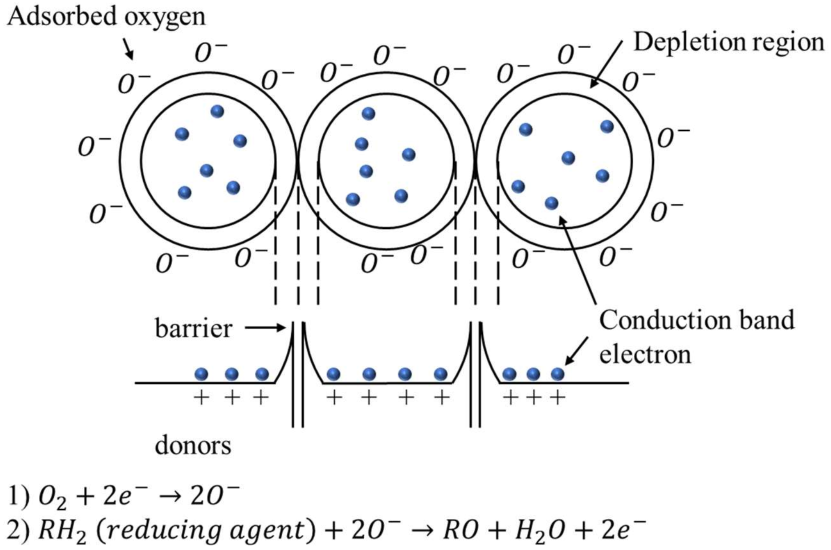

Figure 4 Schematic diagram for a conduction process controlled by a Schottky barrier mechanism.

2.2 Performance elements of the gas sensor

2.2.1 Sensitivity

Gas sensitivity is the most important parameter in gas sensors, and many researchers are working with interest to increase the sensitivity. Gas sensitivity is defined as the change in resistance of the gas sensor when the existing gas is exposed to the target gas to be detected. When the gas detection layer reacts with the target gas, this change in resistance changes the resistance of the existing gas (Resistance air, R_a) to the resistance of the target gas (Resistance gas, R_g), or blocks the target gas after the reaction ends, It refers to the change in which R_g returns to R_a when is flowed for a certain time. The reaction between the gas sensing layer and the target gas can be measured in equipment that can flow the desired gas at a certain time and amount.

When comparing gas sensing methods, the *n*-type metal oxide semiconductor and the *p*-type metal oxide semiconductor operate in opposite ways. When reacting with the reducing gas, the resistance of the *p*-type metal oxide semiconductor increases, while the resistance of the *n*-type metal oxide semiconductor decreases. In general, the method of quantifying gas sensitivity can be calculated as $S = R_a / R_g$ for reducing gases (CO, H_2, NH_3) or $S = R_g / R_a$ for oxidizing gases (O_2, NO_2) [8, 9]. Gas sensitivity is affected by the material in the gas sensing layer, catalyst and operating temperature [10]. In addition, in the gas detection reaction, a large amount of oxygen ion molecules are adsorbed on the surface of the gas detection layer to cause a reaction with the target gas, so a large surface area is also required to increase gas sensitivity [11].

2.2.2 Response and recovery time

Looking at how a gas sensor works, the speed at which the sensor has to detect the gas is very important. The reaction time refers to the time required for the sensor to react to the gas when the concentration value of the gas is 0 to a specific concentration value. The reaction time τ generally refers to the time it takes for the sensor to reach 90% of the resistance when a gas reaction occurs according to a change in gas concentration. The reason is that when exposed to the target gas in the presence of the existing gas, the resistance of the sensor increases or decreases very quickly according to the reaction, and then enough time is required to reach a certain value.

Like the response time, the recovery time is also important, because the recovery time is closely related to the reproducibility that is maintained even after repeated use in a situation where the sensor is constantly circulated for a long time. The recovery time refers to the time it takes to recover to 10% of the initial resistance value after the gas reaction is over and before the sensor resistance reacts according to the change in the concentration from a specific concentration value to 0. The response time and recovery time are very important parameters in gas sensors, and the shorter the time, the better the sensor criteria, so adjusting them greatly depends on the commerciality of the gas sensor.

2.3 Effects of catalysts and additives

Most oxide semiconductor gas sensor devices are manufactured by adding a noble metal catalyst (Pd, Pt, Ag, etc.) or a metal oxide additive (CuO, WO_3, etc.). Devices in which noble metals are added to oxide semiconductors usually have a small conductivity in air because the size of the Schottky barrier is increased. Therefore, when detecting gas, its sensitivity increases. Another major function of the catalyst is that it lowers the temperature at which the highest sensitivity is achieved and shortens the reaction time. These catalytic effects are explained by the chemical function (spill over) and the electrical function (Fermi energy control) [12]. Figure 3-5 shows the model diagram of the operation of the two functions.

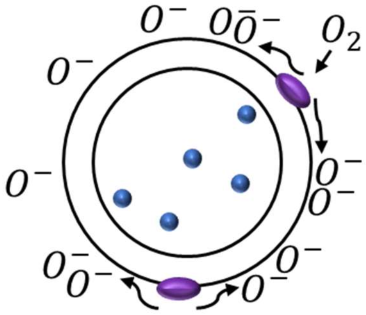

Figure 5. Schematic diagram illustrating the catalytic function: spill over.

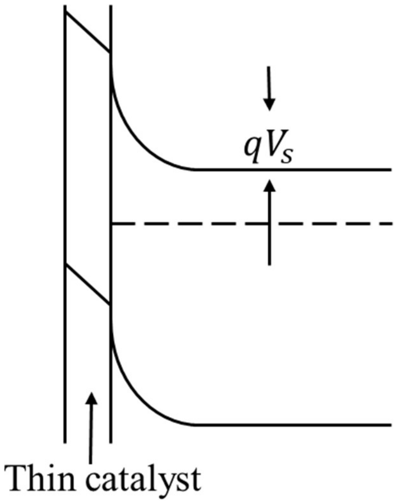

Figure 6. Schematic diagram illustrating the catalytic function: Fermi energy control.

Figure 3 shows the chemical function. In other words, molecular oxygen is decomposed into atomic oxygen by the catalytic action of the catalytic metal, and the decomposed oxygen flows to the surrounding base material due to the difference in concentration thereof (spillover effect). Therefore, the height of the barrier increases because more atomic oxygen is adsorbed to the base material in the form of anions. As such, the metal catalyst can increase the sensitivity of the gas and increase the selectivity according to the type of target gas by selective spill over of target gas. In the case of Pt, it is difficult to say that it becomes an oxide by adsorption of oxygen (the sublimation temperature of PtO is about 500°C), so it is accepted as having a chemical function. If this is expressed by the chemical formula, as below:

In case of typical model without catalyst, the chemical reaction is expressed

$$O_2 + 2e^- \rightarrow 2O^- \tag{10}$$

$$RH_2(reducing\ agent) + \ 2O^- \rightarrow RO + H_2O + 2e^- \tag{11}$$

Since the chemical reaction in the presence of a Pt catalyst is expressed as follows, it can be seen that a larger change in resistance is shown in the presence of a catalyst.

$$2Pt + O_2 \rightarrow 2Pt - O \tag{12}$$

$$O + e^- \rightarrow O^- \tag{13}$$

Figure 4 shows the Fermi energy control. In case of SnO_2, the work function of Pd is 4.8eV, which is greater than the electron affinity (4.5eV) of the SnO_2 semiconductor. At this time, when the precious metal and the semiconductor come into contact on the surface, electrons are transferred from the semiconductor to the metal, thereby forming an electron depletion layer and a Schottky barrier on the surface of the semiconductor. Here, when oxygen is adsorbed on the surface of the catalytic metal in the form of anion or forms an oxide, more electrons are transferred from the semiconductor to the catalytic metal, so that the barrier height of the semiconductor surface is further increased. However, in order to obtain the effect of electrical functions over the entire area of the particles by adding a small amount of catalyst, the distribution of these catalysts must be well controlled to be uniform as shown in Fig. 5.

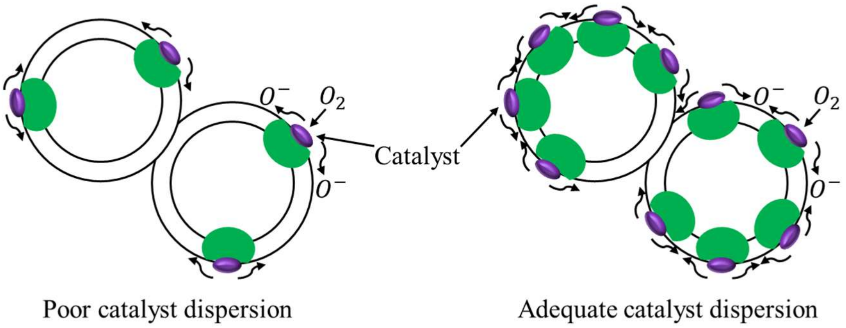

Figure 7 Schematic diagram illustrating the catalytic function: adequate catalyst dispersion.

For oxide semiconductor devices, additives are used for various purposes [13]. The first function of the additive is the function of changing the microstructure of the device. In other words, it regulates the shape and content of pores by controlling the degree of small crystals, adjusts and stabilizes the size of the particle-to-particle contact, changes the sensitivity and stabilizes the change in characteristics according to the history of use. As an example, there is a case in which CaO is added to SnO_2 to maintain a fine particle size to improve sensitivity. Second, the additive affects the bonding structure between electrons in the device and promotes or suppresses semiconductorization, thereby changing the sensitivity characteristics. This includes increasing the sensitivity by adding Al to SnO_2 or reducing the sensitivity by adding Sb. However, despite the aforementioned research efforts of catalysts and additives, there are still many theoretical deficiencies, so the structure of the sensor parent material, catalytic activity of the sensor material, thickness of the membrane, electrode structure, and measurement optimality must be considered together [14].

2.4 References

[1] A. M. Azad, S. A. Akbar, S. G. Mhaisalkar, L. D. Birkefeld, K. S. Goto, Solid-State Gas Sensors: A Review, J. Electrochem. Soc. 139 (1992) 3690-3704.

[2] M. N. Rumyantseva, A. M. Gaskov, N. Rosman, T. Pagnier, J. R. Morante, Raman surface vibration modes in nanocrystalline SnO_2: correlation with gas sensor performances, Chem. Mater. 17 (2005) 893-901

[3] L. Madler, T. Sahm, A. Gurlo, J.-D. Grunwaldt, N. Barsan, U. Weimar, S.E. Pratsinis, Sensing low concentration of CO using flame-spray-made Pt/SnO_2 nanoparticles, J. Nanopart. Res. 8 (2006) 783-796

[4] Y.C. Lee, H. Huang, O.K. Tan, M.S. Tse, Semiconductor gas sensor based on Pd-doped SnO_2 nanorod thin films, Sens. Actuators B, 132 (2008) 239-242

[5] Z. K. Horastani, S. M. Sayedi, M. H. Sheikhi, E. Rahimi, Effect of silver additive on electrical conductivity and methane sensitivity of SnO_2, Mater. Sci. Semicond. Process. 35 (2015) 38-44

[6] N. Bhardwaj, A. Pandey, B. Satpati, M. Tomar, V. Gupta, S. Mohapatra, Enhanced CO gas sensing properties of Cu doped SnO_2 nanostructures prepared by a facile wet chemical method, Phys.Chem.Chem.Phys. 18 (2016) 18846

[7] S. C. Chang, Thin-film semiconductor NO_x sensor, IEEE Transactions on Electron Devices, 26 (1979) 1875-1880.

[8] C. Wang, L. Yin, L. Zhang, D. Xiang, R. Gao, Metal oxide gas sensors: sensitivity and influencing factors, Sensors 10 (2010) 2088-2106

[9] K. Wetchakun, T. Samerjai, N. Tamaekong, C. Liewhiran, C. Siriwong, V. Kruefu, A. Wisitsoraat, A. Tuantranont, S. Phanichphant, Semiconducting metal oxides as sensors for environmentally hazardous gases, Sens. Actuators B 160 (2011) 580-591

[10] N. Yamazoe, G. Sakai, K. Shimanoe, Oxide semiconductor gas sensors, Catal. Surv. Asia 7 (2003) 63-75

[11] M. Tiemann, Porous metal oxides as gas sensors, Chem. Eur. J. 13 (2007) 8376-8388

[12] S. Matsushima, Y. Teraoka, N. Miura, Y. Yamazoe, Electronic interaction between metal additives and tin dioxide intin dioxide-based gas sensors, Jpn. J. Appl. Phys. 27 (1988) 1798-1802.

[13] N. Yamazoe and N. Miura, Chemical Sensor Technology Vol.4, (1992) 19-42, Kodansha Ltd. and Elsevier, Tokyo.

[14] Y. Shimizu, Y. Nakamura, M. Egashira, Effects of diffusivity of hydrogen and oxygen through pores of thick film SnO_2-based sensors of their sensing properties," Sensors and Actuators B. 13 (1993) 128-131.

CHAPTER 3. SENSOR ARRAY FOR DETECTING VARIOUS KINDS OF GASES

3.1 Introduction

Various metal-oxide semiconductors, such as ZnO, TiO_2, CuO, SnO_2, and WO_3, have been extensively studied as novel candidates for various energy and sensing-device applications owing to their excellent chemical, mechanical, electrical, and optical properties [1-3]. In particular, various nanostructures of the materials, such as nanoparticles, nanowires, nanorods, and nanobelts, with very high surface-to-volume ratios have been used to create extremely sensitive and selective sensor platforms. Various sensing materials, catalysts, and sensor designs, such as temperature gradients, have been employed to differentiate the sensor properties of multi-component arrays and fabricate highly selective sensors. The use of various materials as a variable for sensor arrays is particularly effective due to the different chemical processes occurring on the sensor surface when target gases were adsorbed. However, the number of the sensing materials is limited by high costs, complicated processes, and low yields. Recently, a nanowire junction array platform comprising ZnO and CuO was suggested to reduce the number of the materials; furthermore, the adsorbed gas molecules modify the potential barrier height formed at the junctions and the carrier transport inside the materials [4].

Thus far, many bottom-up approaches for preparing metal-oxide nanowires, such as chemical vapor deposition, physical vapor deposition, hydrothermal process, and electrochemical deposition, have been studied and are well established [5-17]. However, these approaches are mainly limited by the difficultly in integrating planar substrates to exploit their useful functional properties. This requires compatible surfaces and molecules, but there are fewer tools available for manipulating the molecules and atoms. The transfer process to foreign substrates was not efficient for fabricating the sensor arrays. A specific procedure for the large-scale assembly of functional transducers is desirable for assuring that they are reliably integrated into functional devices. The most promising approach appears to be the hydrothermal process, supported by rational engineering of the substrate. It is also suitable for fabricating many types of large-scale nanowires for highly selective sensor arrays. By using this technique, a sensor array consisting of ZnO, CuO, and TiO_2 nanowires was reported, in which the TiO_2 nanowires were constructed by coating TiO_2 onto ZnO and then etching the ZnO; however, nanowire growth was limited to the specific area heated by the applied voltage, and this technique is not suitable for growing large-area nanowires [18].

Here, a highly selective gas detection strategy based on the continuous iteration method of various nanowires growth at a wafer level by using hydrothermal process was described. The order of the nanowire growth was determined by the aqueous precursor solution pH, the growth temperature, and the seed layers. The five kinds of nanowire (WO_3, TiO_2, SnO_2, CuO, and ZnO) could be grown on desired locations of the 2-inch substrate without any interaction between them. The nanowires were decorated by the silver (Ag) nanoparticles, in which the catalytic processes occurring on the Ag depended on the barrier height formed at the interface, thereby, paving the way to a useful strategy for making sensor array. The sensor array with palladium (Pd) and Ag nanoparticles was tested for the ability to distinguish between the hydrogen, carbon monoxide, and nitric dioxide with detection limits ranging from sub-ppm to ppm levels, enabled the gas responses to be separated into three classes using linear discriminant analysis.

3.2 Experimental details

3.2.1 Fabrication of a full wafer-scale gas sensor

The nanowire growth on wafer-scale substrates were carried out by depositing a seed layer at desired locations using a conventional lithography technique and then using a hydrothermal method. The growth order was determined by the precursor solution pH, the growth temperature, and the seed layer (Fig. 6). WO_3 nanowires were grown by depositing a WO_3 film using radio-frequency (RF) reactive sputtering with 80 W of RF power, 10 sccm of Ar and 10 sccm of O_2 at an operating pressure of 4 mTorr. This was followed by annealing at 400°C for 5 min under flowing nitrogen gas. The substrates were then placed floating face-down on the growth solution (0.1 M sodium tungstate, 3 M hydrochloric acid (HCl) and 0.1 M ammonium sulfate in deionized water (DI) (adjusted to pH 2.0) and heated in an oven at 180°C for 4 h. TiO_2 nanowires were grown by similar methods, but the TiO_2 film sputtering was conducted with 16 sccm of Ar and 4 sccm of O_2 with the other conditions unchanged; the TiO_2 nanowires were also annealed at 400°C for 5 min under flowing nitrogen gas to enhance their growth. Actually, the growth was so sensitive to the growth temperature (Fig. 7). The nanowires were grown in a solution of 30 ml of DI, 30 ml of HCl and 2 ml of titanium butoxide at 130°C for 7 h [7]. The sputtering conditions for the SnO_2 film were the same as those for the TiO_2 film. The substrates were then kept in the growth solution (100 ml of DI, 0.001 M of tin chloride, 0.1 M of urea, and 5 ml of HCl) at 90°C for 24 h [20]. The sputtering conditions for the CuO seed layer was same as those for the WO_3 film, except 50 W of RF power was used. The nanowires were grown in the growth solution (1:1 ratio of copper nitrate and hexamethylenetetramine (HMTA) 25 mM) at 90°C for 5 h [10]. The ZnO nanowire growth procedure is established and the growth conditions are gentle so that other nanowires are not significantly damaged during ZnO nanowire growth.

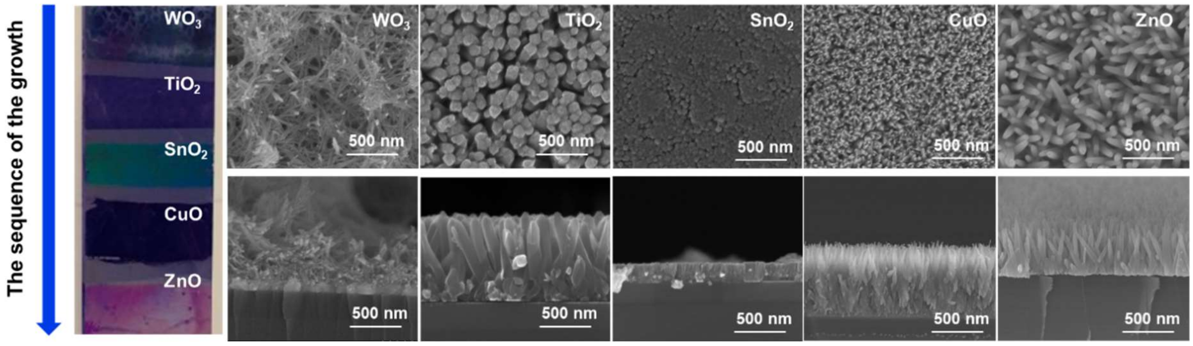

Figure 8. The nanowire growth sequence determined by considering the aqueous precursor solution pH,

the growth temperature, and the seed layers. The five nanowire types could be grown on desired locations of the 2-inch substrate with no interactions between them.

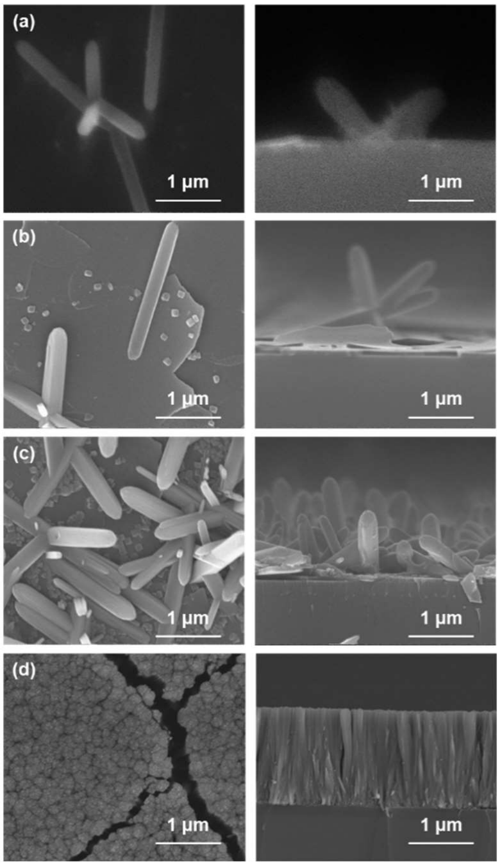

Figure 9. TiO_2 nanowires grown on various seed layers that were annealed at (a) 200, (b) 300°C, (c) 400°C, and (d) 500°C.

Three nanowire types (TiO_2, CuO, and ZnO) were used for the sensor arrays, which were grown according to the aforementioned growth order (Fig. 8(a)). After they were grown, Ti/Au (20/200 nm) and Ni/Au (20/200 nm) were deposited as electrodes on the n- and p-type nanowires, respectively. 3 nm thick (mass thickness) Pd and Ag films were separately deposited by electron beam evaporation at a base pressure of 5.0×10^{-6} Torr through a shadow mask, which was appropriately placed over linear sets of the three sensors elements to functionalize the nanowires. The fully fabricated samples were annealed for 1 min by rapid thermal annealing under a nitrogen atmosphere at 450°C to improve the ohmic contact between the nanowire and metal electrodes. The annealing process also made the metallic film to be aggregated to nanoparticles.

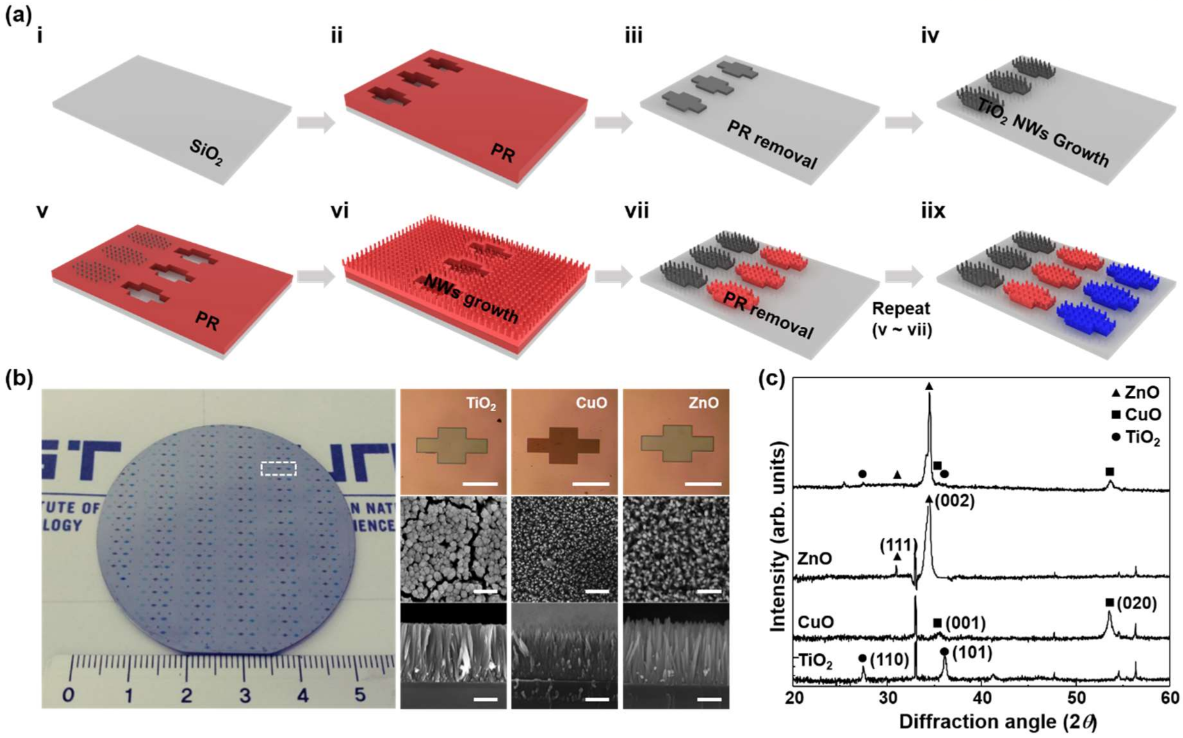

Figure 10. (a) Schematic diagrams of the fabrication process for gas sensors based on the multiple nanowires. The nanowire growth order was determined by considering the aqueous precursor solution pH, the growth temperature, and the seed layers. (b) Image of the TiO_2, CuO and ZnO nanowires grown at a 2-inch wafer scale. Scale bars in the image and SEM images are 500 μm and 500 nm, respectively. (c) X-ray diffraction spectra of TiO_2, CuO, ZnO nanowires, and the multiple nanowires. There was no secondary peak in the spectra of the multiple nanowires.

3.2.2 Material characterizations

All nanowires were characterized by field-emission scanning electron microscopy (FE-SEM) and X-ray diffraction (XRD). XRD diffraction patterns were recorded on a Normal X-ray diffractometer (Bruker, Germany) using Cu Kα radiation with a wavelength of 1.5418 Å. To measure the electrical characteristics of the various metal-oxide nanowires, a bias sweep from −5 to 5 V was applied across the electrodes at 250°C and the resistance of each nanowire was measured using a Keithley 2636A source measurement unit.

3.2.3 Response test

The sensors were placed in a reaction chamber and exposed to pulses of one of three gases at various partial pressures (H_2: 100 ppm, CO: 50 ppm, and NO_2: 10 ppm), which were entrained in a flowing air gas with a flow rate of 2000 sccm. The gas sensors were measured in a probe chamber (~125 cm^3) equipped with an electrical measurement system, a vacuum and temperature controlling system, and a precisely controlled gas flow system. Pure air was introduced between the pulses. Each of the analytes gases had a low humidity concentration of approximately 2.2×10^{-6} (μmol/mol) and total hydrocarbon (THC) level of zero. The current was measured using a Keithley 2636A source measurement unit. All three produced similar results and the radar chart of each yielded points that localized in similar regions of parameter space for the three test gases. The results reported herein were obtained in a long series of experiments from one of the devices. A 1 V bias was applied to the electrodes. The sensor response is defined as $S = (R_g\text{-}R_a/R_a)$ in which R_g and R_a are the steady-state resistance values measured with the analyte gas added to the air stream, and the air stream alone, respectively.

3.3 Results and discusstion

3.3.1 Wafer-scale vertically-aligned five kinds of nanowires

The resultant sensor array is shown in Fig. 8(b). The product consists of TiO_2, CuO, and ZnO nanowires arrays, which were successfully grown on the 2-inch wafer-scale SiO_2/Si substrate by a continuous iteration method (Fig. 8(a)). According to the growth conditions, TiO_2 nanowires were grown on the wafer first because of the high growth temperature (~130°C) and very low pH value (~ 0.7); under these conditions, other nanowires are easily removed by etching. TiO_2 nanowires growth was significantly affected by the seed (Figs. 7 and 9). As described in the experimental section, the TiO_2 seed was prepared by RF sputtering at room temperature, which was followed by a high-temperature annealing process. At temperature below 400°C, the seed was easily peeled-off and very few nanowires with submicron diameters were observed. Further increasing the temperature to 500°C yielded a greater number of nanowires and decreased the nanowire diameter to approximately 90 nm (Fig. 7). There were no TiO_2 nanowires on the substrate surface without a seed layer, which is very important for fabricating sensor arrays that comprise various materials. CuO and ZnO nanowires were also grown on a seed layer only (Fig. 9). The mean nanowire widths were measured for a representative number of nanowires and determined by SEM, which were: 88.2 ± 10.7, 56.3 ± 10.2, and 43.9 ± 5.9 nm, respectively. The nanowire growth time was controlled to produce nanowires approximately 1 μm in length.

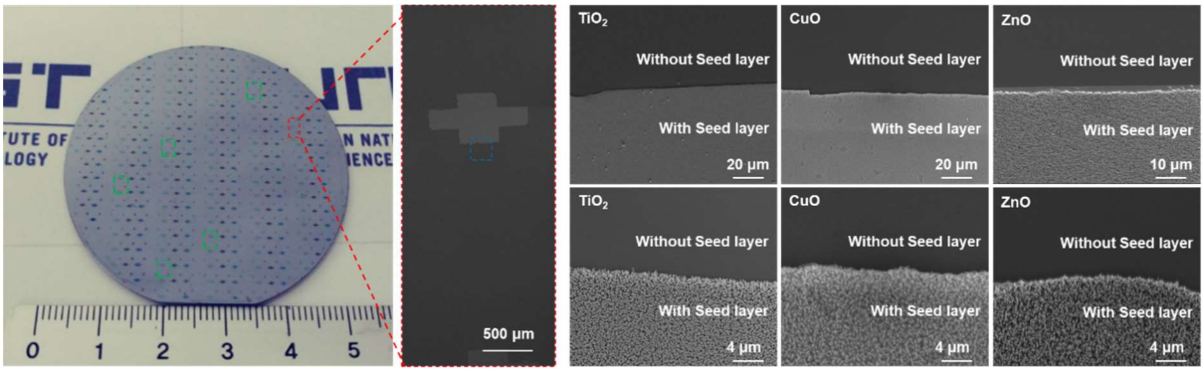

Figure 11. Image of the multiple TiO_2, CuO, and ZnO nanowires that were hydrothermally grown at a wafer level. The nanowires were grown on the seed layers. There were no nanowires on the region without the seeds, which is shown in the SEM images.

XRD analysis in Fig. 8(c) revealed four clear representative peaks at 27.5°, 36.1°, 34.4°, and 53.6°, which corresponded to crystal phases at (110) and (101) for TiO_2, (002) for ZnO, and (020) for CuO, respectively. Thus, all diffraction peaks were indexed as a mixture of tetragonal (TiO_2), monoclinic (CuO), and hexagonal (ZnO) phases. Compared with the individual nanowire XRD data, no remarkable shift in the diffraction peaks or change in FWHMs were detected: ~0.36°–0.37° for TiO_2 (101) peak, ~0.36°–0.37° for CuO (020) peak, and ~0.11°–0.12° for ZnO (002) peak. Therefore, this process is quite useful for growing various nanowires on any large-scale wafer without producing any interaction between the nanowires.

The detailed crystal structure of TiO_2, CuO, and ZnO nanowires were also investigated by low- and high-magnification TEM images of nanowires. Low-magnification TEM images of both representative nanowires and selected area diffraction (SAED) patterns taken from the same sample are shown in Fig. 10. The TiO_2 and ZnO nanowires are shown to be single crystalline with tetragonal and hexagonal structure, and growth directions along [1 1 0], and [0 0 2] axis, respectively. However, CuO nanowires shows a polycrystalline structure, having mainly (0 0 1) and (1 1 0) planes at the surface. Fig. 11 also shows the Energy dispersive X-ray spectrscopy for the compositional analysis. It reveals that each nanowires are composed of Ti, Cu, Zn, and O, respectively. This supports the XRD results above indicating that no interaction between nanowires.

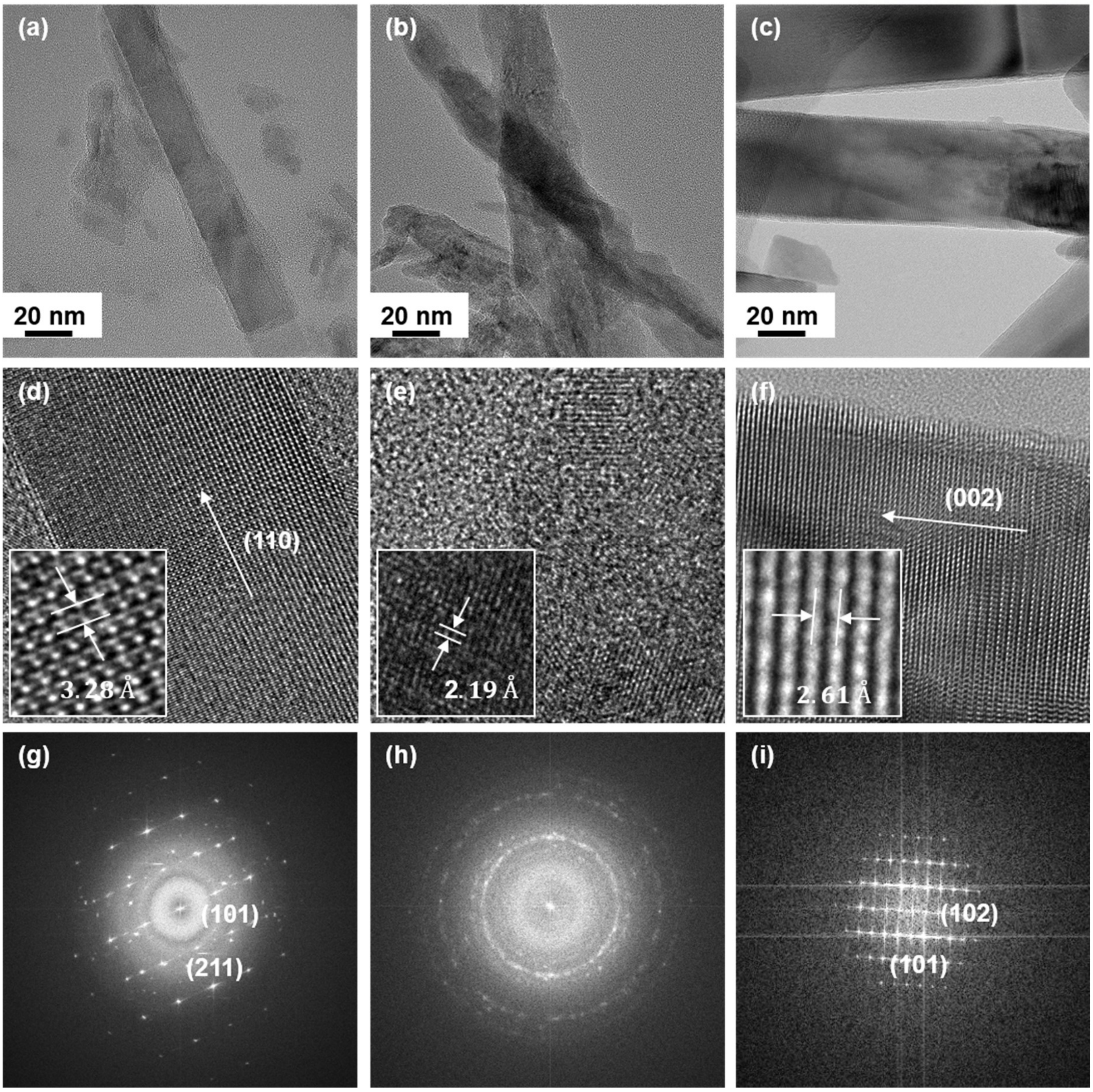

Figure 12. Low- and high-magnification TEM images and the selected area diffraction patterns for TiO_2 (a, d, g), CuO (b, e, h), and ZnO (c, f, i), respectively. The TiO_2 and ZnO nanowires are single crystalline with tetragonal and hexagonal structure, along [1 1 0] and [0 0 2] direction, respectively. CuO nanowires has a polycrystalline structure.

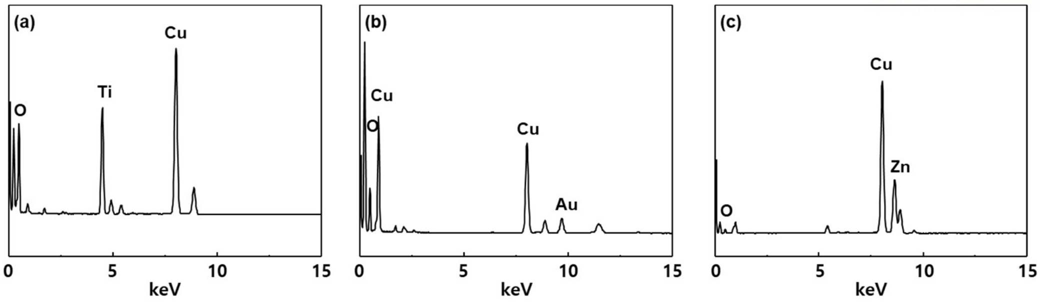

Figure 13. Energy dispersive X-ray spectroscopy (EDS) of (a) TiO_2, (b) CuO, and (c) ZnO nanowires.

These results suggest that wet-chemical approaches, such as a hydrothermal process, may be appropriate for growing various nanowire types on single wafer-scale substrate; however, a vacuum-assisted physical vapor process is sometimes needed for preparing the seeds for each nanowire. One of many advantages is that conventional semiconductor processing techniques, such as photoresist patterning, can be used in the approach to grow the various nanowire types on single substrates since most nanowires can be grown under low temperatures (< 200°C). Here we carefully optimized the nanowire growth order by considering the nanowire growth conditions, such as precursor solution pH, the growth temperature, and the seed layers. By using this wet-chemical approach, many different types of nanowires could be grown, such as WO_3 and SnO_2. The WO_3, TiO_2, SnO_2, CuO, and ZnO nanowires were grown on a single substrate (Fig. 6).

3.3.2 Gas-sensing properties of nanowire arrays

Ti/Au (20/200 nm) and Ni/Au (20/200 nm) electrodes were deposited onto *n*-type (TiO_2 and ZnO) and *p*-type (CuO) nanowires, respectively, to investigate the influence of various gases (H_2, CO, and NO_2) on carrier transport inside the nanowires (Fig. 12(a)). To enhance the ohmic contact characteristics at the metal-semiconductor interface, the wafer was annealed for 1 min at 450°C under a nitrogen atmosphere. All I-V curves were clearly linear so all contacts were considered to be ohmic and the resistance of each nanowires in the air was measured at 250°C, as shown in Fig. 12(b). The resistance of ZnO, TiO_2, and CuO nanowires were measured to be 0.4, 1.06, and 0.93 MΩ, respectively. In *n*-type metal oxides, the current passing through ZnO nanowires was 2.7-fold greater than that passing through TiO_2 nanowires, which may be attributed to the larger ionization energy (~ 0.33 eV) [21] between the shallow donors and the edge of the conduction band of TiO_2 compared to ZnO (~0.05 eV) [22]. The resistance of the CuO and *n*-type is also comparable, which is helpful for obtaining reliable sensing properties. It is generally supposed that the holes flow through the hole accumulation layer formed at the oxide surface in *p*-type metal oxides. The ohmic I-V curve of CuO nanowires indicates that the surface layer is well-formed. The ionization energy of approximately 0.22 eV indicates that the electrical properties of CuO nanowires are reasonably reliable [23].

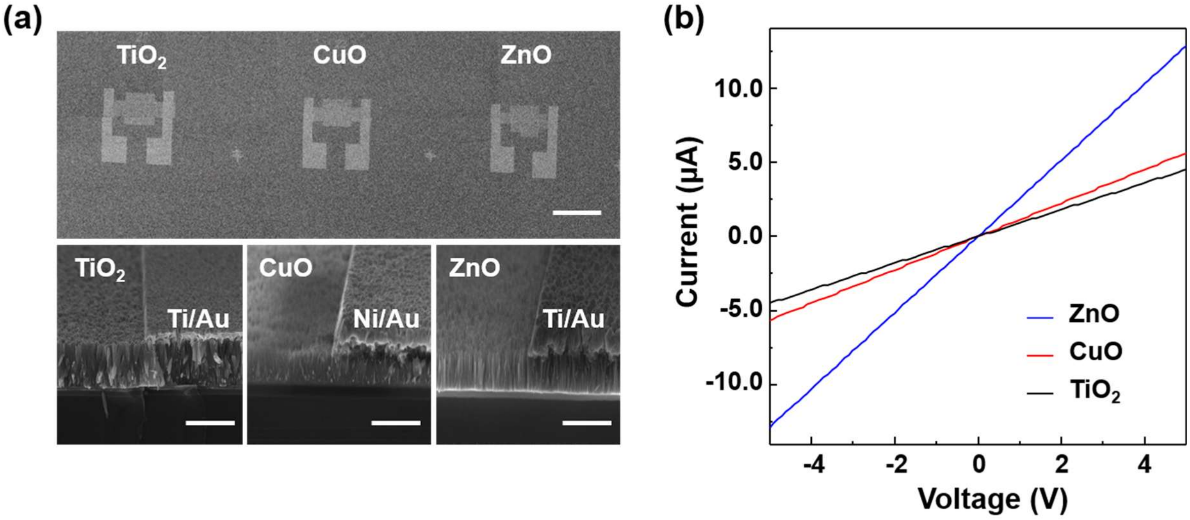

Figure 14. (a) SEM image of the fabricated gas sensor. Scale bar in the image is 500 μm. The cross-sectional SEM image was obtained after Ti/Au and Ni/Au metallization. The scale bar is 500 nm. (b) Representative I-V curves measured at 250°C, which show the typical ohmic behaviors.

The responses of the pristine ZnO, TiO_2, and CuO nanowires toward H_2, CO, and NO_2 gases of 100, 50, and 10 ppm, respectively, measured at 250°C, were plotted in Fig. 13. The measured *S* values on pristine ZnO nanowires were -0.12, -0.07, and 0.47 respectively. For the TiO_2 nanowires, the sensitivities toward the gases are relatively low, compared with those of ZnO nanowires. In case of p-type CuO nanowires, they showed the opposite responses toward H_2 gas compared to *n*-type nanowires, as reported previously [4, 24] for H_2, CO, and NO_2 gases, the measured *S* values were 0.1, 0.1, and -0.01, respectively. In general, the adsorbed oxygens from background air create more near-surface holes and the hole accumulation layer was formed in CuO nanowires. The hydrogen-induced change of the thickness in the hole accumulation layer at the CuO nanowire surface was reported as gas sensing mechanism [24, 25]. The sensing performance can be explained via the crystallinity and morphology of the materials. The CuO has a flake-like morphology which can help the transport of the gases through the nanowires, compared with the other nanowires having nanorod-type morphology. However, the CuO is polycrystalline, in which gas molecules adsorbed on the surface diffuse into its interior, and then are likely to cover the grain boundaries. This will produce the electron depleted layers at the interfaces of two adjacent grains, eventually generating a potential barrier for electrons to flow. This will decrease the sensing performance.

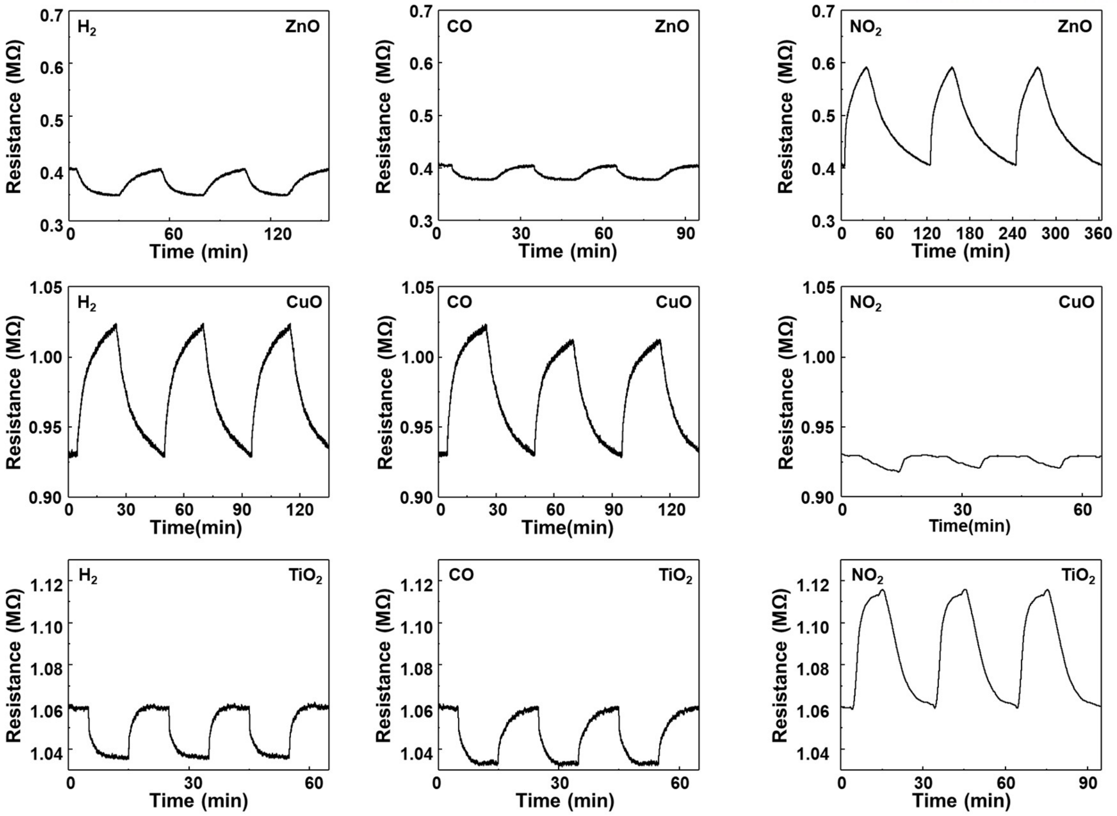

Figure 15. Representative sets of resistance measured as a function of time at an applied source-drain voltage of 1 V for ZnO, CuO, and TiO_2 nanowires toward H_2, CO and NO_2 gases at 250°C.

The responses of the ZnO, TiO_2, and CuO nanowires decorated with Ag nanoparticles at 250°C toward H_2 gas with concentration of 100 ppm are plotted in Fig. 14, compared with pristine nanowires. The size of the nanoparticles ranged from 8 to 11 nm. The measured S values on pristine ZnO, TiO_2, and CuO nanowires were -0.12, -0.024, and 0.1, respectively, as shown in Fig. 13. As the Ag nanoparticles were decorated, the S value in ZnO nanowires increased to -0.14, showing an increase by approximately 17 %, while the TiO_2 nanowires did not show any significant change, as shown in Fig. 14(d). This indicates that Ag acted as a catalyst to increase the sensitivity in only ZnO nanowires. This may be explained via electron transport across the interfaces between the Ag and the nanowires. In a background stream of air at 250ºC, it is believed that the oxygen molecules were absorbed on the surface of the Ag, forming various adsorbed oxygen ions (O_2^-, O^-, and O^{2-}) at the surface, thus, the Ag was oxidized to AgO_x. When it was exposed to H_2 gas, the hydrogen molecules reacted with the oxygen ions to form water and electron. At the AgO_x–ZnO interface, an ohmic contact was formed, as shown in Fig. 15(a) [26]. This promotes the formation of adsorbed oxygen ions (O_2^-, O^-, and O^{2-}) at the Ag surface and gas oxidation via the enhanced electron exchange between the Ag and the ZnO. However, the barrier height at the interface of the AgO_x-TiO_2 is so high (~ 1.5 eV), which makes the transport of electrons across the interface quite difficult, as shown in Fig. 15(b) [27, 28]. This resulted in no significant change in resistance of TiO_2 by the decoration of the Ag.

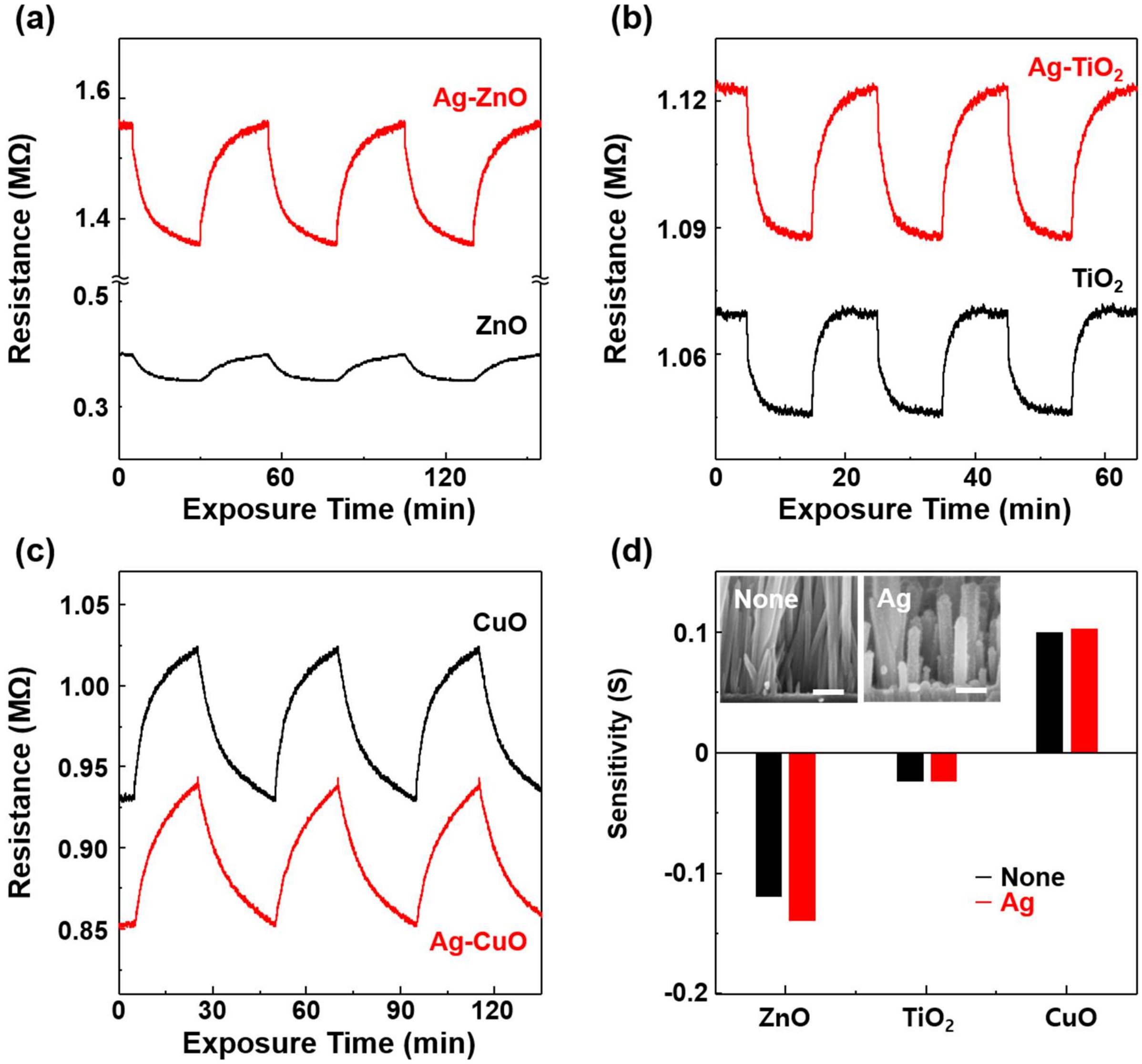

Figure 16. Representative sets of resistance measured as a function of time at an applied source-drain voltage of 1 V for (a) ZnO, (b) TiO_2, and (c) CuO nanowires with Ag nanoparticles toward H_2 gas at 250°C. (d) Representative values of the sensitivities of the sensor toward the three gases. Cross section-view SEM images of ZnO nanowires without and with Ag nanoparticles. (scale bar is 200 nm)

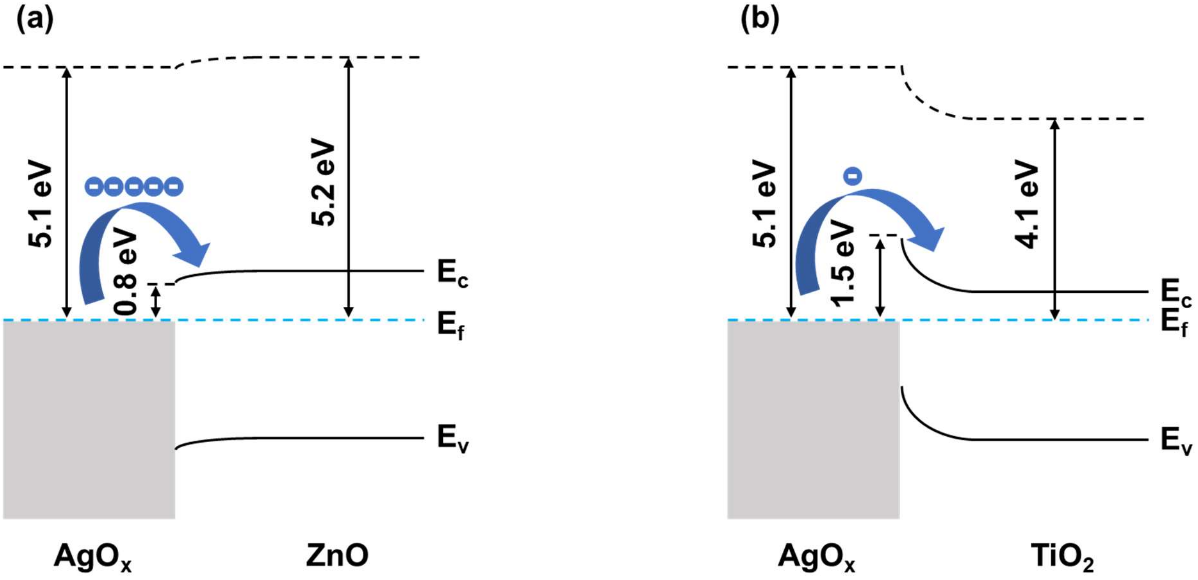

Figure 17. Energy band diagram at the interface of (a) AgO_x/ZnO and (b) AgO_x/TiO_2

In case of p-type CuO nanowires, when it was decorated with Ag, exposed to the H_2 gas, electrons would be formed by the reaction with the oxygen ions, increasing the resistance of the CuO due to the electron transfer process to CuO, followed by the electron-hole recombination process in CuO. The AgO_x would also be reduced to Ag by the reaction, thereby, bending more the energy band near the interface of CuO [24, 25]. Thus, the resistance of the CuO nanowires will increase by the two effects, leading to the increase of the sensitivity by 7 % due to the Ag decoration. The sensitivity can be also controlled by the thickness of the Ag, that is, the density of the Ag nanoparticles, as reported before [6]. Figs. 16(a) and 16(b) show the sensing performance of Ag-decorated CuO nanowires toward H_2 gas as a function of the thickness of the Ag. When 5 nm-thick Ag was decorated and annealed, it showed the highest sensitivity, ~ 40 % enhancement compared with the pristine CuO nanowires. However, further increase in the thickness of the Ag decreased the sensitivity, because the nanoparticles were too large to being catalytically active at the interface, as shown in Fig. 16(c).

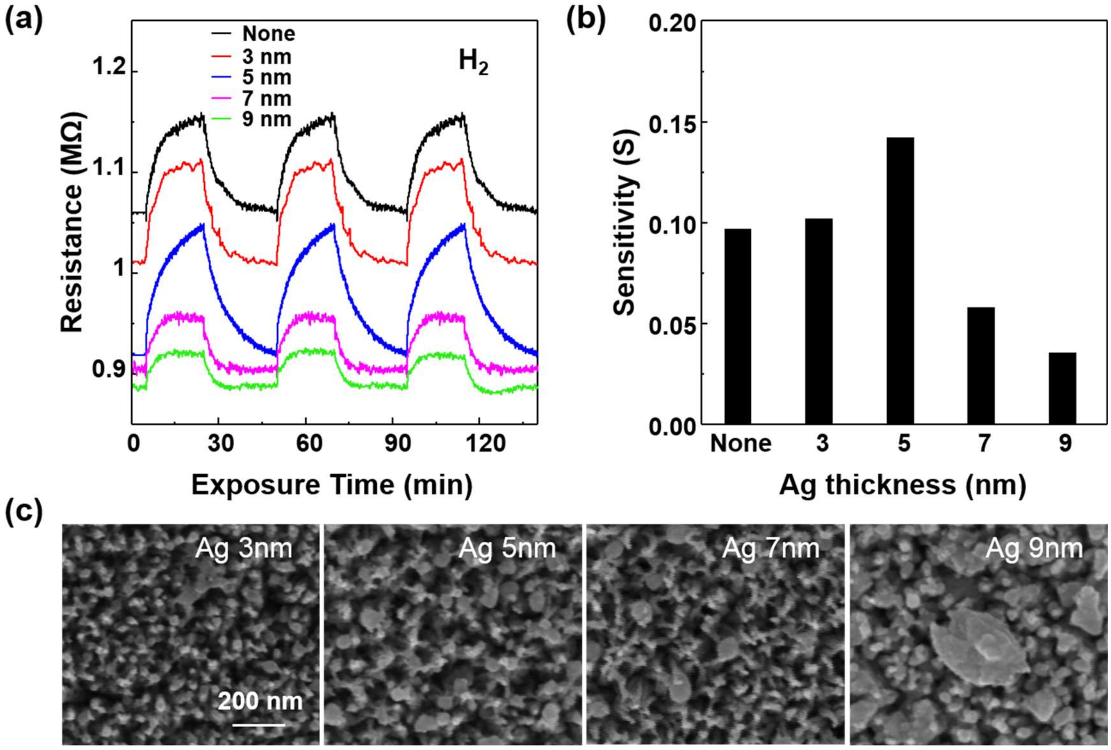

Figure 18. (a) Resistance change and (b) sensitivities of CuO nanowires and Ag-decorated CuO nanowires as a function of the thickness of the Ag film. (c) SEM images of Ag-decorated CuO nanowires as a function of the thickness of the Ag film.

When decorated with Pd, the sensitivities toward the hydrogen significantly increased to -0.47, -0.20, and 0.26 in ZnO, and TiO_2, and CuO nanowires, respectively, as shown in Fig. 17. The hydrogen molecules were known to be dissociated on the Pd nanoparticle surface, and then underwent fast diffusion into the metal oxides, resulting in increased sensitivities [29]. Fig. 18(a) also shows the resistance responses of pristine, Pd-decorated, and Ag-decorated ZnO nanowires toward CO and NO_2 gases with concentration of 100, 50, and 10 ppm, respectively. For the CO and NO_2 gases, the measured S values on pristine ZnO nanowires were -0.07 and 0.47, respectively. After the Pd nanoparticles were decorated, the S values increased to -0.24 and 8.69, respectively. As the Ag nanoparticles were decorated, the S values also increased -0.09 and 0.63, respectively. Although the increased sensitivities were not as large as many as those produced by the Pd nanoparticles, the catalytic effects of the Ag were also observed in the gases. The similar tendency for sensitivities of TiO_2 and CuO nanowires toward the gases were observed in Figs. 18(b) and 18(c).

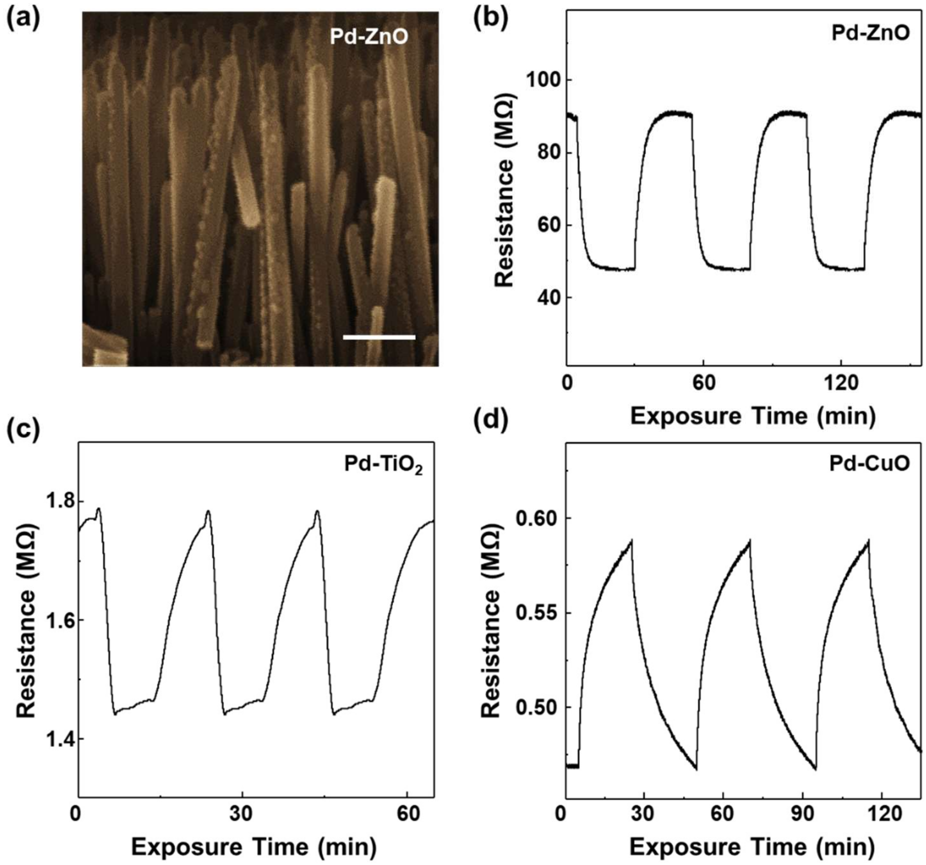

Figure 19. (a) SEM image of Pd nanoparticle coated ZnO nanowires. Representative sets of resistance measured as a function of time at an applied source-drain voltage of 1 V for (b) ZnO, (c) TiO_2, and (d) CuO nanowires decorated with Pd metal nanoparticles in the presence of H_2 gas at 250°C.

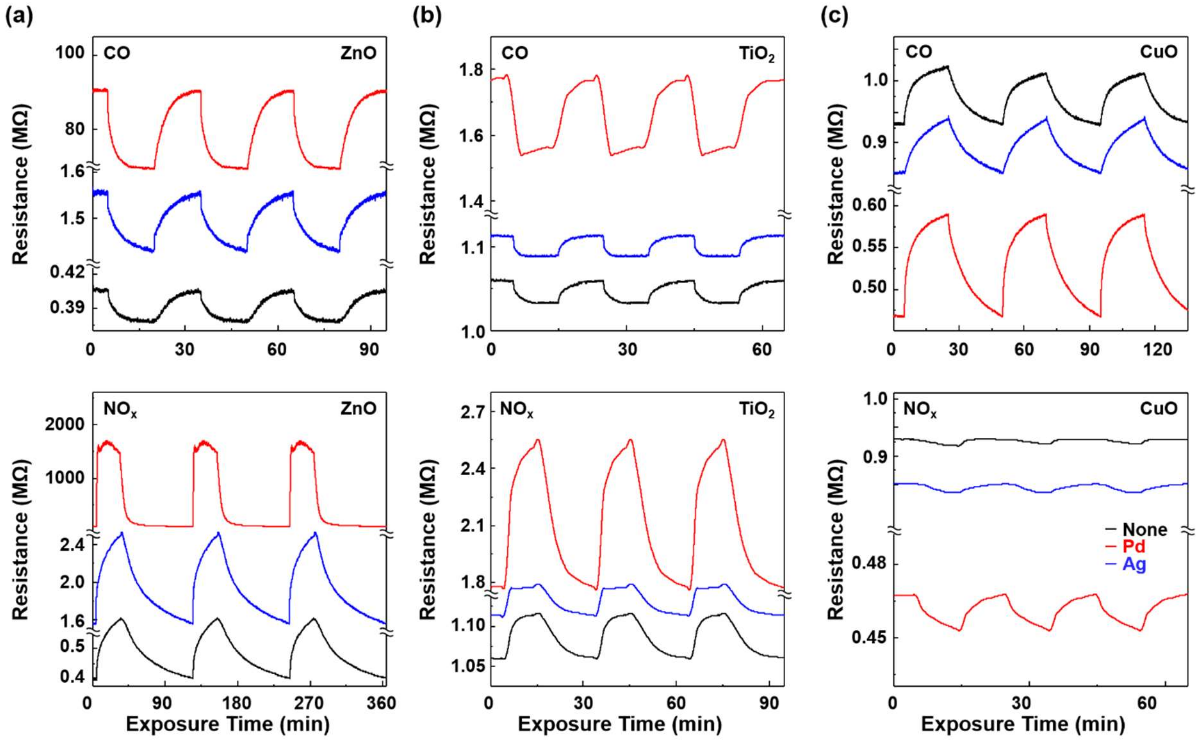

Figure 20. Representative sets of resistance measured as a function of time at an applied source-drain voltage of 1 V for (a) ZnO, (b) TiO_2, and (c) CuO nanowires with Pd and Ag nanoparticles toward CO and NO_2 gases at 250°C.

To investigate the discriminating power of the sensor array of the Fig. 19(a), radial plots of the H_2, CO, and NO_2 gas responses measured from the nine sensor elements were obtained (Fig. 20). The sensitivities toward the three gases for *n*-type nanowires sensors yielded the opposite responses, compared with those of sensor consisting of *p*-type nanowires. Furthermore, there was a clear difference in the catalytic activity between Ag-decorated ZnO and TiO_2 nanowires. It is noted that each gas sensor in the sensor array has a specific sensitivity pattern for different gases, which enables the various gas species to be discriminated. The aggregate data for the sensor array, which was processed using linear discriminant analysis (LDA), enabled the gas response of the sensor arrays to the three gases to be separated into three classes (Fig. 19(b)). LDA analysis was carried out using a commercial code (XLSTAT 2018, Addinsoft, France). According to the data separation, H_2, CO, and NO_2 could be identified at a 95% confidence level by the sensor array described here.

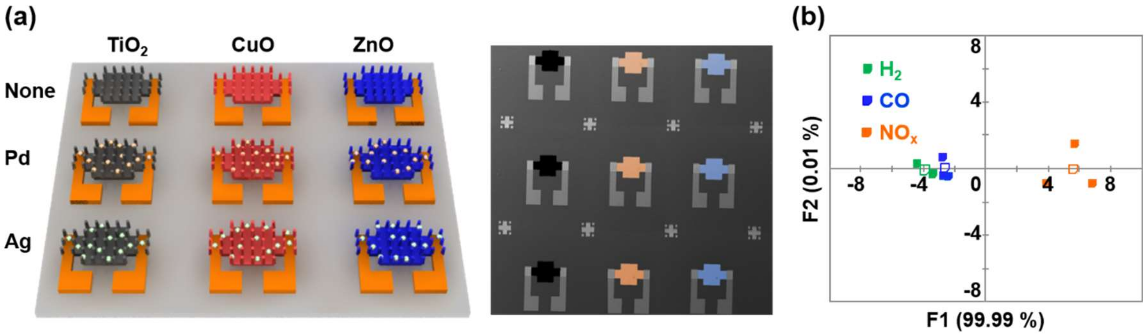

Figure 21. (a) Schematic of 3 × 3 sensor arrays and the SEM image. (b) The result of an LDA analysis of the sensitivities obtained for the sensor arrays.

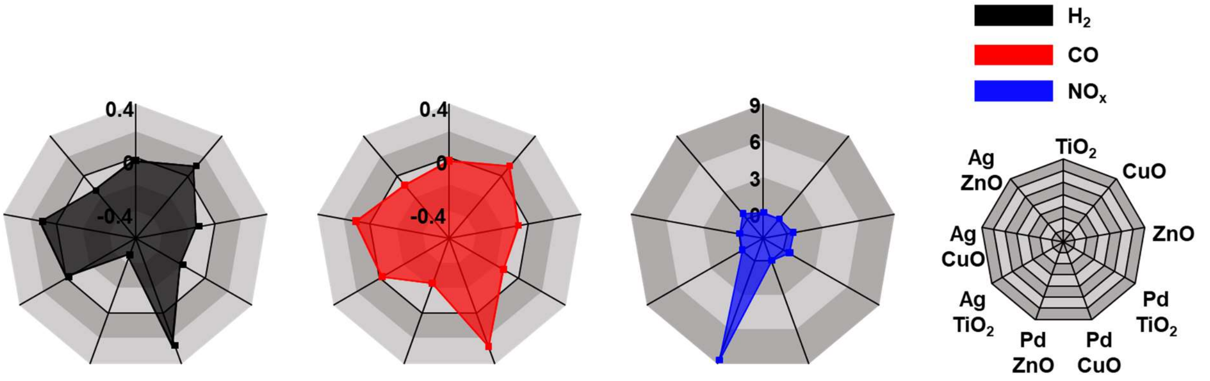

Figure 22. Radar charts of gas sensitivity for H_2, CO and NO_2 gas species, which was measured from the nine sensor elements of the sensor arrays shown in Figure 14a.

The gas detection limits of the Pd-nanoparticle-decorated nanowires for H_2, CO, and NO_2 were obtained by measuring the gas responses as a function of the gas concentration (Figs. 21 and 22). At low gas concentrations, the sensitivities exhibited almost a linearly response with increasing concentrations. Thus, such arrays can be used for the continuous and reliable real-time gas monitoring at such low concentrations. However, further increases in the gas concentration beyond certain concentrations decreased the gradient of the linear regression line between detector response and gas concentration. The decreased sensitivities at high concentration were reported to be due to the degradation of carrier mobility, which is attributed to the scattering effects of adsorbed gas molecules [30]. Although the sensitivities were measured at concentrations ranging from 1 to 100 ppm, depending on the gas type, it was believed that the gases could be detected at very low concentrations (ppm scale). The limit of detection (LOD) was calculated based on the standard deviation of the response of the curve and the gradient of the calibration curve at concentrations close to the LOD according to the formula. The LOD for each gas were 5.4 ppm of H_2 gas for ZnO nanowires, 2.15 ppm of CO gas for TiO_2 nanowires, and 0.47 ppm of NO_2 gas for ZnO nanowires. The standard deviation of the response can be determined based on the standard deviation of y-intercepts of regression lines.

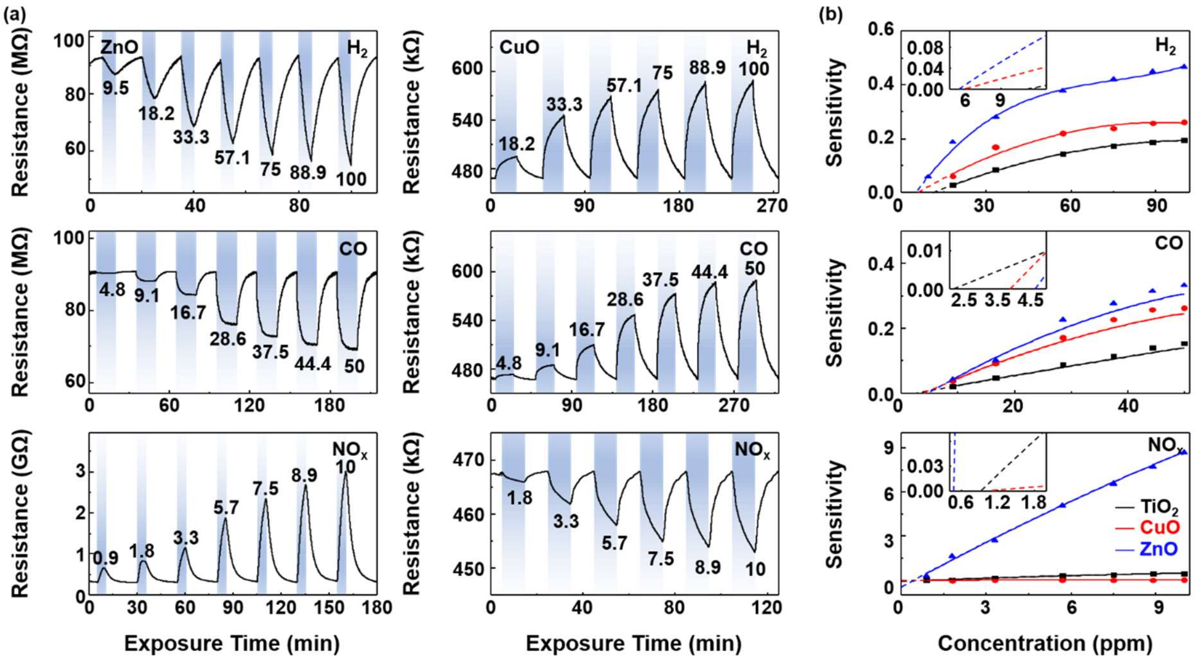

Figure 23. Limit of Detection (LOD) tests for each nanowire decorated by Pd nanoparticles for each gas at 250°C

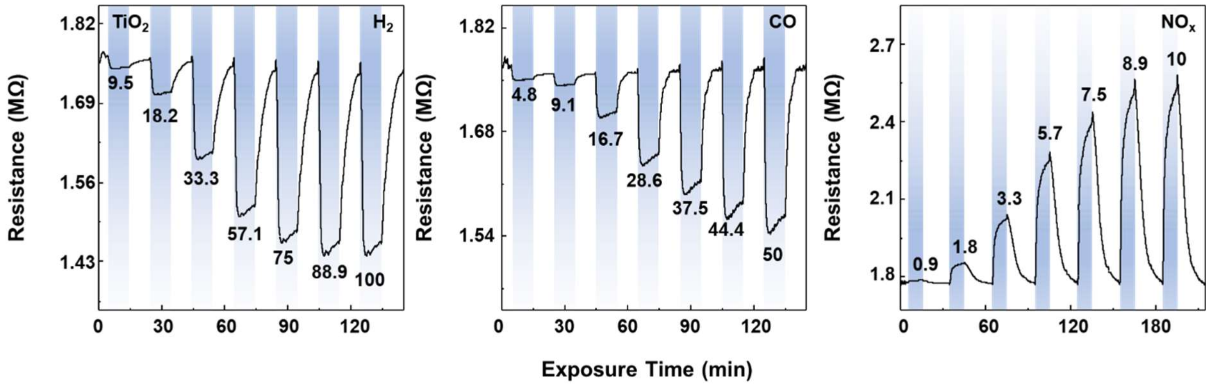

Figure 24. Limit of Detection (LOD) test for the Pd-decorated TiO_2 nanowires for each gas.

Finally, we evaluated the sensor response to the three gases in the presence of water vapor in relative humidity of 50, 70, and 90 %), plotted in Fig. 23. As the moisture was introduced, the sensitivities from all sensors were decreased and the resistance of the samples were also decreased. The decrease in resistance in air and sensitivity is known to be related with the water poisoning reaction occurring at the surface [31-34]. The LDA results also showed that the ability to distinguish the gases got worse. In particular, CO and H_2 gases were not distinguished. In the reaction of the gases, they react with oxygen ions, releasing one electron. In dry environements, quite enhanced sensing performance by the catalytic effects of the Pd at the surface is obtained in H_2 gas. However, in wet condition, the water molecules react the oxygen ions to produce hydroxide ions, decreasing the number of the oxygen ions, as below;

$$H_2O + O^{2-} \rightarrow 2OH^-$$

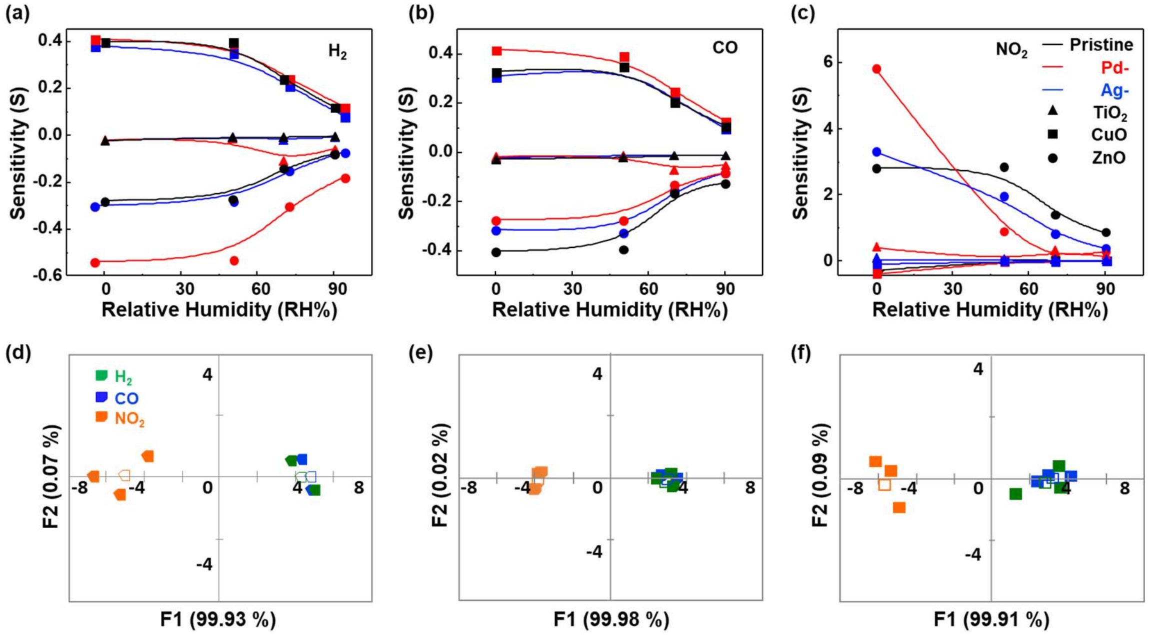

Figure 25. Gas response to (a) H_2 100 ppm, (b) CO 50 ppm, (c) NO_2 10 ppm as a function of relative humidity from 50 to 90 %. The LDA analysis of the sensitivities obtained for the sensor arrays with relative humidity of (d) 50%, (e) 70%, and (f) 90%.

Thus, the catalytic properties of the palladium nanoparticles were critically deteriorated by water poisoning. It is believed that this is why the H_2 and CO gases are not distinguished in the LDA analysis as the humidity increases.

3.4 Conclusion

In summary, a facile continuous iteration method of various kinds of nanowires (WO_3, TiO_2, SnO_2, CuO, and ZnO) growth at a wafer level using a hydrothermal process was described. Although the hydrothermal growth of the individual nanowires is not novel, the selective-area growth of various kinds of nanowires at a wafer-level is essential for commercializing the use of metal oxides for sensor applications. Here, the nanowire growth order was determined by considering the aqueous precursor solution pH, the growth temperature, and the seed layers. Thus, the five kinds of nanowire could be grown on desired locations of 2-inch substrate with no interactions between them.

With the various kinds of nanowires on a single substrate, the high-selectivity detection of H_2, CO, and NO_2 gases was represented by decorating Pd and Ag nanoparticles, and fabricating 3 × 3 sensor arrays consisting of ZnO, TiO_2, and CuO nanowires. The increase in gas sensitivities that can be achieved by Pd-decoration, and the enhanced gas selectivity by *n*-type and *p*-type metal oxides has previously been established. The Ag decoration made the nanowires have different gas responses by modifying the catalytic process occurring on the nanowires and on the Ag in two ways: (1) by the modification of the electron exchange rate across the Ag/metal-oxides interface depending on the magnitude of the barrier height. (2) by the change of the carrier concentration due to the band-bending changes at the metal-oxides. Thus, the gas responses of Ag-decorated TiO_2 nanowires was distinct from those of Ag-decorated ZnO nanowires. The Ag nanoparticles on CuO nanowires were also catalytically active depending on the size of the nanoparticles. Finally, the sensor arrays showed an enhanced discriminating power for resolving between H_2, CO, NO_2 with the limits of detection ranging from sub-ppm to ppm concentrations.

3.5 References

[15] R.S. Devan, R.A. Patil, J.H. Lin, Y.R. Ma, O[Devan, 2012 #14]ne-dimensional metal-oxide nanostructures: recent developments in synthesis, characterization, and applications, Advanced Functional Materials 22 (2012) 3326.

[16] T. Zhai, X. Fang, M. Liao, X. Xu, H. Zeng, B. Yoshio, D. Golberg, A comprehensive review of one dimensional metal-oxide nanostructure photodetectors, Sensors 9 (2009) 6504.

[17] Z.L. Wang, X.Y. Kong, Y. Ding, P. Gao, W.L. Hughes, R. Yang, Y. Zhang, Semiconducting and piezoelectric oxide nanostructures induced by polar surface, Advanced Functional Materials 14 (2004) 943.

[18] W.J. Park, K.J. Choi, M.H. Kim, B.H. Koo, J.L. Lee, J.M. Baik, Self-Assembled and Highly Selective Sensors Based on Air-Bridge-Structured Nanowire Junction Arrays, ACS Applied Materials & Interfaces 5 (2013) 6802-6807.

[19] Q. Kuang, C. Lao, Z.L. Wang, Z. Xie, L. Zheng, High-sensitivity humidity sensor based on a single SnO_2 nanowire, Journal of the American Chemical Society. 129 (2007) 6070.

[20] J.M. Baik, M. Zielke, M.H. Kim, K.L. Turner, A.M. Wodtke, M. Moskovits, Tin oxide-nanowire-based electronic nose using heterogeneous catalysis as a functionalization strategy, ACS Nano 4 (2010) 3117–3122.

[21] O. Alev, E. Sennik, N. Kilinc, Z.Z. Ozurk, Gas Sensor Application of Hydrothermally Growth TiO_2 Nanorods, Procedia Engineering 120 (2015) 1162-1165.

[22] J. M. Baik, M. H. Kim, C. Larson, C. T. Yavuz, G. D. Stucky, A. M. Wodtke, M. Moskovits, Pd-Sensitized Single Vanadium Oxide Nanowires: Highly Responsive Hydrogen Sensing Based on the Metal-Insulator Transition, Nano Lett. 9 (2009) 3980-3984.

[23] Q. Wan, Q.H. Li, Y.J. Chen, T.H. Wang, X.L. He, J.P. Li, C.L. Lin, Fabrication and ethanol sensing characteristics of ZnO nanowire gas sensors, Applied Physics Letters 84 (2004) 3654–3656.

[24] S. Xia, H. Zhu, H. Cai, J. Zhang, J. Yu, Z. Tang, Hydrothermally synthesized CuO based volatile organic compound gas sensor, RSC Advance 4 (2014) 57975.

[25] J.X. Wang, X.W. Sun, Y. Yang, H. Huang, Y.C. Lee, O.K. Tan, L. Vayssieres, Hydrothermally grown oriented ZnO nanorod arrays for gas sensing applications, Nanotechnology 17 (2006) 4995–4998.

[26] W. Kim, M. Choi, K. Yong, Generation of oxygen vacancies in ZnO nanorods/films and their effects on gas sensing properties, Sensors and Actuators B 209 (2015) 989–996.

[27] V. Gurav, M.G. Gang, S.W. Shin, U.M. Patil, P.R. Deshmukh, G.L. Agawane, M.P. Suryawanshi, S.M. Pawar, P.S. Patil, C.D. Lokhande, J.H. Kim, Gas sensing properties of hydrothermally grown ZnO nanorods with different aspect ratios, Sensors and Actuators B 190 (2014) 439-445.

[28] S. Steinhauer, E. Brunet, T. Maier, G.C. Mutinati, A. Köck, O. Freudenberg, C. Gspan, W. Grogger, A. Neuhold, R. Resel, Gas sensing properties of novel CuO nanowire devices, Sensors and Actuators B 187 (2013) 50-57.

[29] X. Zou, J. Wang, X. Liu, C. Wang, Y. Jiang, Y. Wang, X. Xiao, J.C. Ho, J. Li, C. Jiang, Y. Fang, W. Liu, L. Liao, Rational Design of Sub-Parts per Million Specific Gas Sensors Array Based on Metal Nanoparticles Decorated Nanowire Enhancement Mode Transistors, Nano Letters 13 (2013) 3287-3292.

[30] K. Kang, D. Yang, J. Park, S. Kim, I. Cho, H. Yang, M. Cho, S. Mousavi, K. Choi, I. Park, Micropatterning of metal oxide nanofibers by electrohydrodynamic (EHD) printing towards highly integrated and multiplexed gas sensor applications, Sensors and Actuators B 250 (2017) 574-583.

[31] J. Yeo, S. Hong, G. Kim, I. Park, C.P. Grigoropoulos, S.H. Ko, Laser induced hydrothermal growth of heterogeneous metal-oxide nanowire on flexible substrate by laser absorption layer design, ACS Nano 9 (2015) 6059-6068.

[32] D. Yang, M.K. Fuadi, K. Kang, D. Kim, Z. Li, I. Park, Multiplexed gas sensor based on heterogeneous metal oxide nanomaterial array enabled by localized liquid-phase reaction, ACS Applied Materials & Interfaces 7 (2015) 10152-10161.

[33] J. Zhang, J. Tu, X. Xia, X. Wang, C. Gu, Hydrothermally synthesized WO_3 nanowire arrays with highly improved electrochromic performance, Journal of Materials Chemistry 21 (2011) 5492.

[34] L. Vayssieres, M. Graetzel, Highly Ordered SnO_2 Nanorod Arrays from Controlled Aqueous Growth, Angewandte Chemie International Edition 43 (2004) 3666.

[35] Y. Mi, Y. Weng, Band Alignment and Controllable Electron Migration between Rutile and Anatase TiO_2, Scientific Reports 5 (2015) 11482.

[36] G. Valverde-Aguilar, J.L. Manrı´quez Zepeda, Photoluminescence Studies on ZnO Thin Films Obtained by Sol-Gel Method, Applied Physics A 118 (2015) 1305-1313.

[37] D.O. Scanlon, B.J. Morgan, G.W. Watson, Acceptor Levels in *p*-Type Cu_2O: Rationalizing Theory and Experiment, Physical Review Letters 103 (2009) 096405.

[38] H. J. Kim, J. H. Lee, Highly sensitive and selective gas sensors using p-type oxide semiconductors: Overview, Sensors and Actuators B 192 (2014) 607-627.

[39] J. Tan, M. Dun, L. Li, J. Zhao, X. Li, Y. Hu, G. Huang, W. Tan, X. Huang, Self-template derived CuO nanowires assembled microspheres and its gas sensing properties, Sensors and Actuators B 252 (2017) 1-8.

[40] S. Ma, J. Xue, Y. Zhou, Z. Zhang, Photochemical synthesis of ZnO/Ag_2O heterostructures with enhanced ultraviolet and visible photocatalytic activity, J MATER CHEM A 2 (2014) 7272-7280.

[41] F.H. Babaei, M.M. Lajvardi, N.A. Sheini, The energy barrier at noble metal/TiO_2 junctions,

Applied Physics Letters 106 (2015) 083503.

[42] F.H. Babaei, Porous silver-TiO_2 Schottky-type chemical sensor fabricated on thermally oxidized titanium, Electronics Letters 44 (2008) 161-162.

[43] C. Wang, L. Yin, L. Zhang, D. Xiang, R. Gao, Metal Oxide Gas Sensors: Sensitivity and Influencing Factors, Sensors, 10 (2010) 2088-2106.

[44] S. Cui, H. Pu, S. A. Wells, Z. Wen, S. Mao, J. Chang, M.C. Hersam, J. Chen, Ultrahigh sensitivity and layer-dependent sensing performance of phosphorene-based gas sensors, Nature Communications 6 (2015) 8632.

[45] N. Yamazoe, K. Suematsu, K. Shimanoe, Two types of moisture effects on the receptor function of neat tin oxide gassensor to oxygen, Sensors and Actuators B 176 (2013) 443–452.

[46] S. Harbeck, A. Szatvanyi, U. Weimar, V. Hoffmann, DRIFT Studies of Thick Film Un-Doped and Pd-Doped SnO_2 Sensors: Temperature Changes Effect and CO Detection Mechanisms in the Presence of Water Vapour, Thin Solid Films 436 (2003) 76–83.

[47] R. G. Pavelko, H. Daly, C. Hardacre, A. A. Vasiliev, E. Llobet, Interaction of Water, Hydrogen and Their Mixtures with SnO_2 Based Materials: The Role of Surface Hydroxyl Groups in Detection Mechanisms, Phys. Chem. Chem. Phys. 12 (2010) 2639–2647.

[48] C. H. Kwak, T. H. Kim, S. Y. Jeong, J. W. Yoon, J. S. Kim, J. H. Lee, Humidity-Independent Oxide Semiconductor Chemiresistors Using Terbium-Doped SnO_2 Yolk−Shell Spheres for Real-Time Breath Analysis, ACS Appl. Mater. Interfaces. 10 (2018) 18886−18894.

CHAPTER 4. INDEPENDENT SENSOR FROM HUMIDITY AND POISONING EFFECT

4.1 Introduction

Chemiresistive sensor platforms consisting of various metal-oxide nanowires with surfaces that have been decorated with metal or metal-oxide nanoparticles have been intensively studied due to their many advantages, such as high sensitivity, high selectivity, and simple fabrication process [1-8]. In principle, surface-chemical processes resulting in a charge exchange between analyte gases and metal-oxides produce resistance changes in the sensors. Because of the high surface-to-volume ratios of the nanowires and the catalytic processes occurring at the surface of the nanoparticles, the platforms could create very sensitive sensors that detect trace amounts of analyte gases. The simple structures also allowed the facile integration of the sensors into small devices, driving the power consumption of the sensors to less than 1 mW [9, 10]. Rapid development of microfabrication techniques and nanotechnologies made them applicable to a wide range of Internet of Things, i.e. sensor network systems consisting of a large number of sensors [11-13].

In the past few decades, there were significant advances that have been made toward commercial metal-oxide sensors. In reality, various metal-oxides such as ZnO, In_2O_3, SnO_2, and TiO_2 had great success in the sensor market place but most of them still did not meet the performance requirements for successful commercialization [14-16]. It is well-known that metal-oxide sensors suffer from degradation processes caused by poisonous interactions that make the surface of the sensors less sensitive to analyte gases. Atmospheric water (H_2O) vapor reacts with the oxygen ions at the surface, decreasing the baseline resistance and reducing the gas response [17, 18]. Hexamethyldisiloxane (HMDSO), the most common representative of organic silicon compound, also deteriorates the sensing performance via the surface-chemical process occurring on the metal and metal-oxide, followed by the formation of a SiO_2 layer [19-22]. For successful commercialization of the sensors, the EN 50194-1 standard, that is, 10 ppm HMDSO over a time period of 40 minutes, should be complied. Up to now, a few papers have reported the degradation mechanism, but there was little reports on the materials' design to reduce or prevent the poisoning effects, and such degradation processes have still remained a problem of practical concern and limit the sensors' growth in the market place[15, 21-25].

In this paper, we suggest a highly stable hydrogen (H_2) detection strategy of the sensors consisting of the Pd nanoparticles-decorated ZnO nanowires in a HMDSO/air environment at 250ºC. The strategy is based on the high dispersion of CeO_2 nanoparticles onto porous reduced graphene oxides (rGO), followed by the coating of the mixture onto the nanowires. The sensor design comes from a fundamental understanding of the degradation mechanism of the sensors by the HMDSO, that is, the decrease of hydroxyl groups and increase of oxygen vacancies by the chemical processes occurring on the surface, and the subsequent formation of the SiO_2 layer. The surface-chemical processes are dramatically affected by introducing the CeO_2 nanoparticles on the nanowires, evident by no change in the resistance of the sensor after HMDSO exposure. The rGO layer is so effective in decreasing the thickness of the SiO_2 layer on the nanowires. Thus, the CeO_2/rGO layer makes the sensors less sensitive to HMDSO exposure, demonstrating excellent long-term stability.

4.2 Experimental details

4.2.1 synthesis of Pd-decorated ZnO nanowires

ZnO nanowires were grown by depositing a ZnO film using radio-frequency (RF) reactive sputtering with 80 W of RF power, 16 sccm of Ar and 4 sccm of O_2 at an operating pressure of 4 mTorr. The substrates were placed floating face-down on the nutrient growth solution (1:1 ratio of zinc nitrate and hexamethylenetetramine (HMTA) 2 mM) and were kept in an oven at 90ºC for 4 h [26]. To enhance the sensing performance, 3 nm thick (mass thickness) Pd films were deposited onto the nanowires through a shadow mask by electron beam evaporation at a base pressure of 5.0×10^{-8} Torr.

4.2.2 Synthesis of CeO_2 nanoparticles and the rGO layer coated with CeO_2 nanoparticles

The rGO layer coated by CeO_2 nanoparticles was prepared by an impregnation method. $Ce(NO_3)_3{\cdot}6H_2O$ purchased at Sigma Aldrich, was used as a precursor for CeO_2 and rGO (Standard graphene, V20-100) was used without modification. The 1 wt% of $Ce(NO_3)_3{\cdot}6H_2O$ and rGO (0.5 g) were dispersed in 50 mL distilled water and 70 mL distilled water, respectively, with vigorous stirring for 1 h. The solutions were mixed and the pH adjusted to 10 by adding NH_4OH. The ultrasonic dispersion was conducted for 1 h and the solution was stirred at 60ºC for 6 h. The mixture was filtered, washed several times to remove unreacted materials and impurities, and dried using a vacuum rotary evaporator. The 1 wt.% of the products were dispersed in ethanol, and spin-coated onto the Pd-decorated nanowires, calcinated at 400ºC for 2 h [27, 28]. In comparison, the pristine CeO_2 nanoparticles without rGO support were prepared by dispersing 1wt% of the $Ce(NO_3)_3{\cdot}6H_2O$ in ethanol and spin-coating onto the Pd-ZnO nanowires, annealed at 400ºC for 2 h. Schematic diagrams for the synthesis process of CeO_2 and CeO_2/rGO using a simple impregnation method are shown in Fig. 24(a).

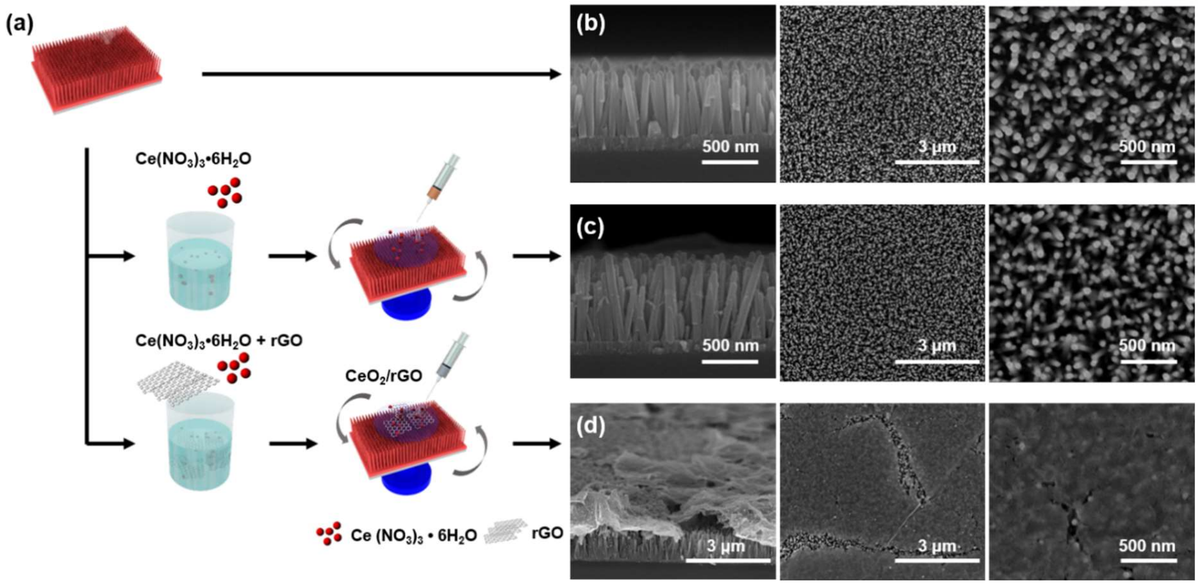

Figure 26. (a) Schematic diagrams of the synthesis process of CeO_2 and CeO_2/rGO using a simple impregnation method. (b-d) SEM images of ZnO nanowires, CeO_2-decorated ZnO nanowires, and CeO_2/rGO-coated ZnO nanowires. From left to right, scale bars in SEM images are 500 nm, 3 µm, and 500 nm.

4.2.3 Material characterization

All nanowires were characterized by field-emission scanning electron microscopy (FE-SEM, FEI, Nova NanoSEM) and X-ray diffraction (XRD). XRD diffraction patterns were recorded on a normal X-ray diffractometer (Bruker, D8 ADVANCE) using Cu Kα radiation with a wavelength of 1.5418 Å. The rGO layer, after impregnation, was analyzed using a transmission electron microscope (TEM, JEOL, JEM-2100F). The ultraviolet photoelectron spectroscopy (UPS, Thermo Fisher Scientific, ESCALAB 250XI) was employed to characterize the element bonding state to confirm the formation of the SiO_2 layer after HMDSO exposure. To measure the electrical characteristics of the various metal-oxide nanowires, a bias sweep from −1 to 1 V was applied across the electrodes at 250°C and the resistance of each nanowire was measured using a Keithley 2636A source measurement unit.

4.2.4 Fabrication of hydrogen sensors and response tests

To fabricate the sensors, Ti/Au (20/200 nm) electrodes were deposited onto ZnO nanowires, then 3 nm-thick Pd film was deposited onto the nanowires in the active region through a shadow mask. The CeO_2 nanoparticles and the CeO_2/rGO mixture were then decorated by the spin-coating process. The fully fabricated samples were annealed for 1 min by rapid thermal annealing under a nitrogen atmosphere at 450°C to improve Ohmic contact between the nanowire and metal electrodes.

The sensors were placed in a reaction chamber and exposed to pulses of one gas at various concentration (H_2: 100 ppm) that were entrained in air gas with a flow rate of 2000 sccm for 40 minutes. The gas sensors were measured in a probe chamber (~125 cm^3) equipped with an electrical measurement system, a vacuum, a temperature controlling system, and a precisely controlled gas flow system. Pure air was introduced between the pulses for 80 minutes. Each of the analyte gases had a low humidity concentration of approximately 2.2×10^{-6} (μmol/mol) and total hydrocarbon (THC) level of zero. To evaluate the sensor response to the gas in the presence of water vapor, the humidity in the chamber was increased to 90 % by introducing wet air into the chamber. The humidity of atmosphere was measured at 25°C just before the wet air was introduced to the sensing chamber. All the gases were controlled using mass flow controllers, as shown in the Fig. 25. Hexamethyldisiloxane (HMDSO) at a concentration of 100 ppm, balanced with air gas, ranging from several minutes to 24 h, was introduced into the chamber to observe the poisoning or deterioration of the sensing material by the silicone vapors. The resistance was measured using a Keithley 2636A source measurement unit at a 1 V bias applied to the electrodes. The sensor response is defined as $S = R_a/R_g$, in which R_g and R_a are the steady-state resistance values measured with the analyte gas added to the air stream, and the air stream alone, respectively.

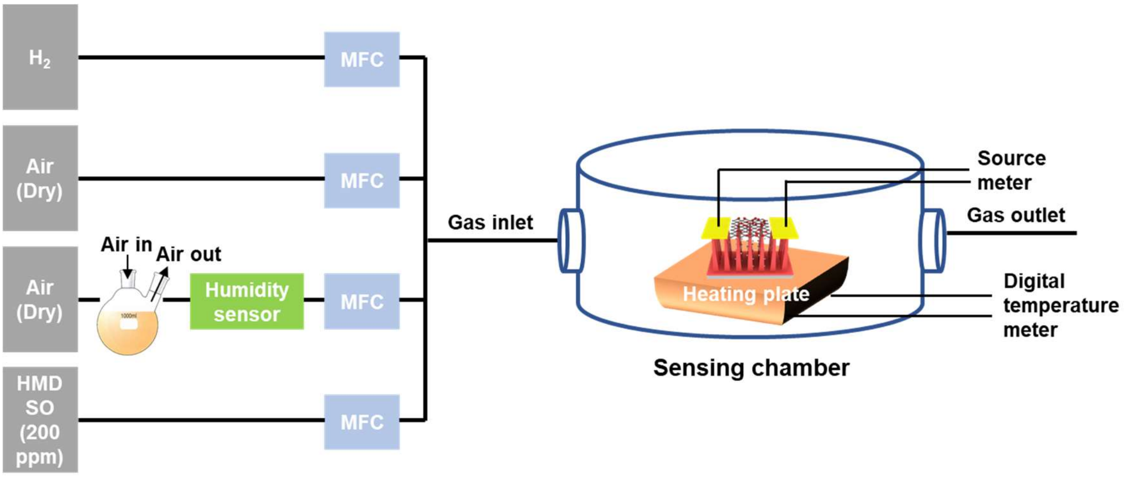

Figure 27. Schematic images of gas supply line to the sensing chamber.

4.3 Results and discussion

4.3.1 Fabrication of a ZnO nanowires-based sensor

As described in the experimental section, the ZnO nanowires were grown via a hydrothermal process. Fig. 24(b) shows that vertically aligned ZnO nanowires were grown on the ZnO seed layer (20 nm) with an average diameter of 52.8 nm and a standard deviation of 5 nm from the statistical analysis on the diameters. In Fig. 24(c), many particles of different sizes ranging from several nanometers to several tens of nanometers were seen to be decorating the side of the nanowires. The top view of the

SEM images showed that there was no agglomeration of the particles on top of the nanowires. This indicates that the surface was hydrophilic enough for the coating of the solution at the side of the nanowires. In the rGO-coated sample, the surface was covered by the rGO layer, on which the CeO_2 nanoparticles were coated. It appears that the nanoparticles were dispersed at the rGO layer. There were a few nanoparticles at the side of the ZnO nanowires, as shown in Fig. 24(d).

XRD experiments were performed to identify the phases in all samples, plotted in Fig. 26(a). The Pd-decorated ZnO nanowires displayed two main peaks corresponding to the ZnO (001) and Pd (111) planes except for Si substrate. When CeO_2 nanoparticles were decorated onto the nanowires, a distinct peak corresponding to the CeO_2 (110) plane was observed. When the concentration of the nanoparticles increased to 3 wt%, the peak intensity was increased and three additional peaks were observed, corresponding to the (200), (220), and (311) planes, as shown in Fig. 27. This clearly shows that the nanoparticles can be indexed as CeO_2. In the rGO-coated sample, the XRD spectrum is similar to that of CeO_2 decorated nanowires. Interestingly, the peak of CeO_2 (110) was shifted by 0.3 ^{o} toward a high diffraction angle, compared to that at CeO_2 decorated nanowires, as shown in Fig. 26(b). This can be explained via the formation of a large number of defects during the interaction with the rGO layer. In addition, due to such interaction between rGO and Ce oxide, the crystal of CeO_2, which is a nonstoichiometric oxide, appears in the form of Ce_2O_3 so that the peak may be shifted [29-31].

Fig. 26(c) shows the TEM image of the CeO_2 nanoparticles-coated rGO layer. It is clearly observed that the rGO layer became quite porous after the impregnation process while the pristine rGO layer without CeO_2 nanoparticles was clean, as shown in the inset. The morphological change of the rGO was investigated by Raman spectroscopy, as shown in Fig. 26(d). In pristine rGO, two representative peaks corresponding to 1350 and 1580 cm^{-1} were observed. By considering the ratio of the relative intensity (I_D/I_G) of the two peaks, many defects seems to be created after the impregnation process. This may be ascribed to the catalytic etching process of the graphene surface through the carbon gasification reaction with Ce ions [29, 32-36]. The size of the nanoparticles ranged over several tens of nanometers due to the role of the anchoring site for the graphene surface, preventing particle aggregation with its binding force.

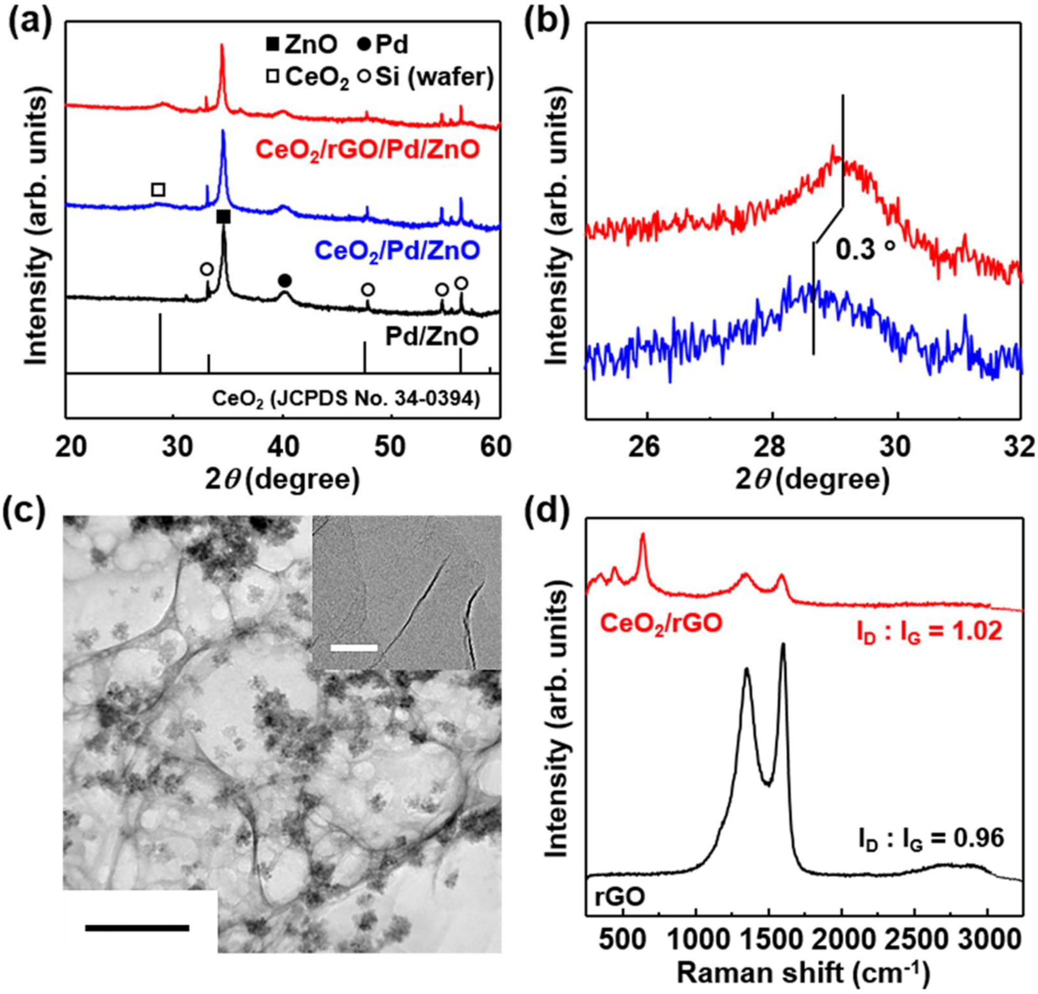

Figure 28. (a) X-ray diffraction spectra of ZnO nanowires, CeO_2-coated ZnO nanowires, and CeO_2/rGO-coated ZnO nanowires. (b) The magnified view of the peak corresponding to CeO_2 (110). (c) Low-magnification TEM image of the CeO_2-coated rGO layer. A TEM image of pristine rGO is also shown in the inset. (d) Raman spectra of pristine rGO and CeO_2 nanoparticles with rGO. The Raman intensity in rGO layer with and without CeO_2 nanoparticles was measured with the laser incident onto the rGO region, and the relative intensity of the two peaks was compared.

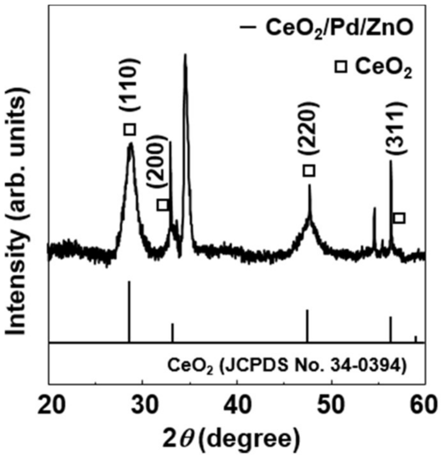

Figure 29. X-ray diffraction spectra of CeO$_2$-decorated ZnO nanowires when the number of nanoparticles increased to 3 wt.%.

4.3.2 Gas-sensing properties of the nanowires-based sensor

Fig. 28(a) shows the fabrication process of the sensors composed of Pd-decorated ZnO nanowires decorated by CeO$_2$ and CeO$_2$/rGO, described above in Experimental section. The cross-sectional SEM images of the Pd-decorated ZnO nanowires, the Pd-decorated ZnO nanowires with CeO$_2$ nanoparticles and the CeO$_2$/rGO mixture near the electrode region are shown in Fig. 28(b). All I-V curves measured at 250ºC were clearly linear, so all contacts were considered to be Ohmic, as shown in Fig. 28(c). The resistance of Pd-decorated ZnO nanowires was measured at 1.6 MΩ. With the decoration of CeO$_2$ nanoparticles, the resistance was increased to 35.9 MΩ. This may be explained via the decrease of oxygen vacancies in ZnO by the supply of oxygen from the CeO$_2$ [37-39]. The introduction of the rGO layer as support also increased the resistance to 42.5 MΩ, indicating that the rGO layer is well-separated, not a continuous planar film and the current does not flow through the rGO layer. It is also well-known that the rGO played as a p-type material, indicating that a *p-n* junction was formed at the interface of the rGO and ZnO (n-type). This will increase the width of the charge-depleted region in ZnO, resulting in an increase of the resistance [40, 41].

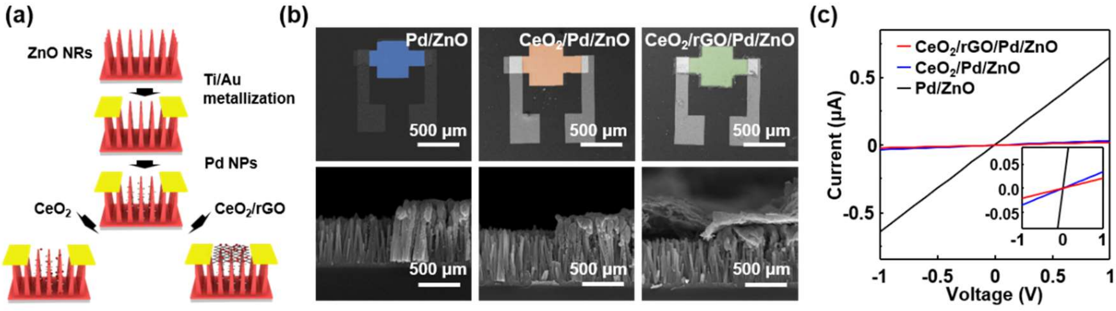

Figure 30. (a) Schematic diagrams of the fabrication process of the sensor composed of Pd nanoparticles

decorated ZnO nanowires decorated by CeO_2 and CeO_2/rGO. (b) Top-view and cross-sectional SEM images of fabricated gas sensors. The scale bars in top-view and cross-sectional images are 500 µm and 1 µm, respectively. (c) Representative I-V curves measured at 250°C.

The responses of the Pd-ZnO nanowires toward H_2 of 100 ppm, measured at 250°C, were plotted in Fig. 29(a). When the H_2 flow was turned on, the resistance rapidly decreased and became nearly saturated after a relatively slow process with a rate constant of ~ 50 $pA \cdot s^{-1}$. The measured S value defined as R_a/R_g, on Pd-ZnO nanowires was about 5.88, demonstrating an increase of the response by 2.4 times, compared with that of the sensor fabricated with pristine ZnO nanowires, as shown in Fig. 30. In general, H_2 molecules are catalytically dissociated on the surface of the Pd, followed by the fast diffusion of H atoms onto the surface, or into the bulk of the ZnO [3, 42]. The H atoms react with the surface oxygens to create hydroxyl groups (OH^-) that can also react with H atoms to produce water, leaving behind oxygen vacancies. The oxygen vacancies were well-known as one of the main donor states in ZnO, thereby increasing the electron concentration at the surface. The H atoms also create the H-based species on the surface or in the bulk of the ZnO associated with another donor states, resulting in an increased electron concentration [42, 43]. The diffusion process of the H atoms into ZnO can explain the slow process via the long diffusion pathway of H atoms into the bulk of the ZnO because the H atom diffusion in ZnO is very slow (the diffusion coefficient is about 2×10^{-11} cm^2/s at 250°C) [44]

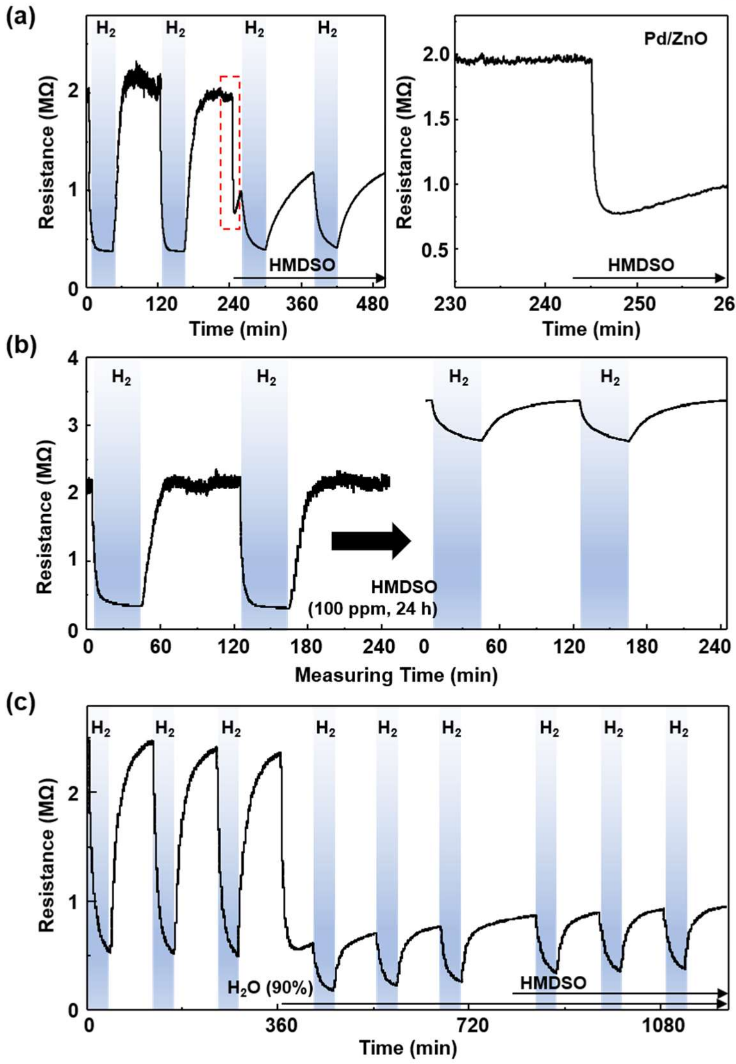

Figure 31. (a) The responses of Pd nanoparticles decorated ZnO nanowires sensors toward H_2 (100 ppm) gas under air and air/HMDSO (100 ppm)), measured at 250°C. The resistance change, when the HMDSO is introduced, is also shown. (b) The responses of Pd-ZnO nanowires sensor toward H_2 (100 ppm) gas before and after the HMDSO exposure for 24 h. (c) The responses of Pd nanoparticles decorated ZnO nanowires sensors toward H_2 (100 ppm) gas under air and air/HMDSO (100 ppm)) at high humidity condition (90 %), measured at 250°C.

When hexamethyldisiloxane (HMDSO, $(O(CH_3)_3Si)_2$) gas of 100 ppm was exposed to the sensor at 250°C, the resistance significantly decreased from 1.9 to 1.0 MΩ, as shown in Fig. 29(a). In general, the siloxane bonds present in HMDSO can hydrolyze in the presence of water, creating Si-OH groups [45, 46]. The generated groups can then react with the hydroxyl groups at the surface of the ZnO, decreasing the amount of the hydroxyl groups. At elevated temperatures, it is expected to produce SiO_2, which may be quite porous and too thin. When decomposed in air, it has generally been considered that the surface oxygens were consumed to produce SiO_2, leaving oxygen vacancies behind. Thus, the surface of the nanowires was modified via the chemisorption of HMDSO, followed by thermal decomposition that decreased the resistance via the increase of oxygen vacancies at the surface [19-22]. With HMDSO exposure, the response also decreased from 5.88 to 2.89. This may be explained via the decrease of the hydroxyl groups at the surface, which decreases the concentration of oxygen vacancies. The formation of SiO_2 will also degrade the catalytic activity of the Pd nanoparticles by decreasing the number of active sites. As the exposure time increased to 24 h, the response was further decreased to 1.21, and the response time and the recovery time also increased 13 to 42.1 min and 12.2 to 53.1 min, respectively, as plotted in Fig. 29(b).

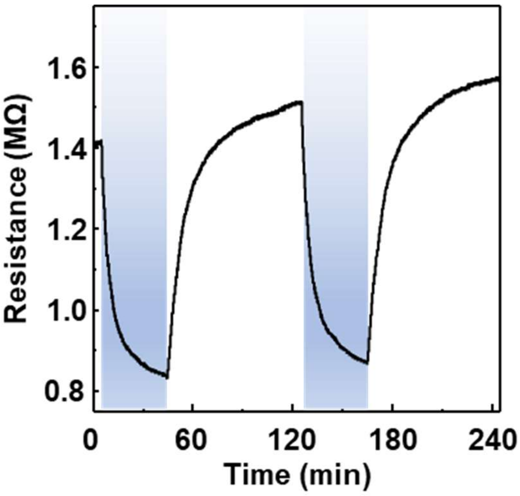

Figure 32. The responses of ZnO nanowires toward H_2 with 100 ppm of air at 250ºC.

For further investigation of the poisoning mechanism by HMDSO exposure, the same experiment was carried out under high humidity conditions. As the humidity increased, the number of absorbed water molecules increased compared to those in low humidity, thereby, more hydroxyl groups would be created. Fig. 29(c) shows the change in resistance of the Pd nanoparticles decorated ZnO sensor in a high humid condition. In the presence of water vapor in relative humidity of 90 %, the resistance decreased from 2.37 to 0.6 MΩ within 30 min. Thus, as moisture was introduced, the resistance of the sensor decreased and the response also decreased. The decrease in resistance in air and response is related to the water vapor chemisorption occurring at the surface using the following equation.

$$O^{-}_{(ad)} + H_2O_{(v)} \rightarrow 2OH_{(ad)} + e^{-} \qquad (1)$$

where $O^{-}_{(ad)}$ is the adsorbed oxygen ions at the surface and $H_2O_{(v)}$ is the water vapor in air. The equation shows the formation of adsorbed-surface hydroxyl groups ($OH_{(ad)}$) from the humidity. When the HMDSO gas of 100 ppm was introduced, there was no change in the resistance or the response. This means that the hydroxyl groups were supplied enough to offset the decrease in hydroxyl groups by the HMDSO reaction, as expected.

To decrease the poisoning effect of HMDSO exposure, CeO_2 nanoparticles were decorated on the nanowires, as described in the experimental section. It is well-known that the cerium oxide is a nonstoichiometric oxide with an excellent ability to store and release oxygens through redox shifts to Ce^{4+}

and Ce^{3+}, thus supplying oxygen to the nanowires. Fig. 31(a) shows the resistance change of the CeO$_2$-decorated sensor with H$_2$ exposure. Compared with Pd decorated ZnO sensor, the response decreased to about 50 %. This may be explained via the degradation of the catalytic activity of the Pd nanoparticles. This weakens the reaction of H atoms with hydroxyl groups to produce an electron. However, when the HMDSO was introduced, no significant change in the resistance was observed. This indicates that the oxygen stored in CeO$_2$ nanoparticles diffused to the surface of the nanowires and was consumed to form the SiO$_2$ [39, 47]. It is also worth noting that the HMDSO exposure to the sensors did not change their response. This implies that the oxygen diffused to the surface produces hydroxyl groups via reaction with the H atoms.

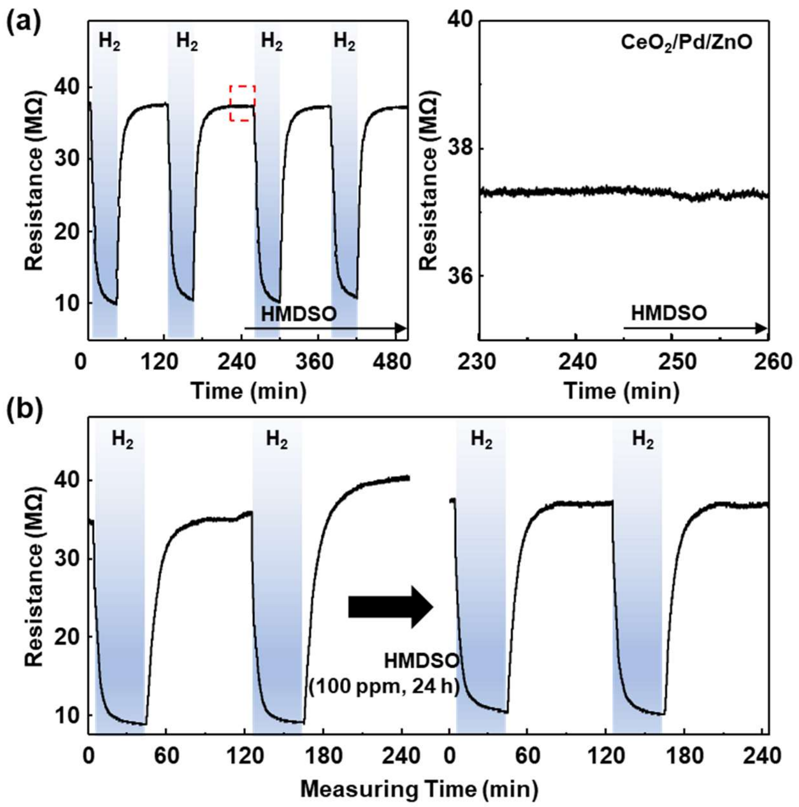

Figure 33. (a) The responses of CeO$_2$-decorated Pd-ZnO nanowires sensors toward H$_2$ (100 ppm) gas under air and air/HMDSO (100 ppm)), measured at 250ºC. The resistance change, when the HMDSO is introduced, is also shown. (b) The responses of CeO$_2$-decorated Pd-ZnO nanowires sensor toward H$_2$ (100 ppm) gas before and after the HMDSO exposure for 24 h.

No significant change in the response implies that the formation of SiO$_2$ did not affect the sensing performance. According to previous reports on the HMDSO-treated sensor, the SiO$_2$ layer was too thin and porous to allow the diffusion of hydrogen molecules through the layer to adsorb them on the surface [24, 48]. However, a few studies by several authors revealed that as HDMSO exposure time increased, the response time and recovery time also increased [15, 19-23, 49]. In Fig. 29(a), after HMDSO exposure on the Pd decorated ZnO nanowires, the response time and the recovery time increased from 13.0 to 31.1 and

12.2 to 41.1 min, respectively. The slow process may be explained via the formation of the SiO_2 layer that would be denser and thicker as the exposure time increased. This will increase the diffusion time of the H_2 molecules from the atmosphere to the surface of the Pd-ZnO. On turning off the H_2 flow, oxygen from the air will also slowly diffuse to the surface, resulting in an increased recovery time. On the contrary, when CeO_2 nanoparticles were decorated, there was no significant change in the response time or the recovery time. However, as the exposure time increased to 24 h, the response time and the recovery time increased from 18.2 to 20.3 min and 11.5 to 12.4 min, respectively. This shows that the CeO_2-decorated sensors do not have long-term stability for the HMDSO poisoning process.

Finally, CeO_2/rGO layer was coated onto the nanowires, annealed at 400°C. Figs. 32 and 33(a) show the resistance change toward H_2 gas of 100 ppm in HMDSO/air environment at 25°C and 250°C, respectively. At 25°C, the resistance was so large (~ MΩ) and there was no significant change in the resistance with H_2 exposure although the resistance decreased a little. This indicates that the current did not flow through the rGO layer. On the other hand, at 250°C, high response of 5.45 was measured. It was clearly observed that there was no change in the response as well as the resistance, as shown in Fig. 34. This experiment was repeated 3 times, also plotted in Fig. 33(a). A further increase in the HMDSO exposure time to 24 h did not also increase the response time or recovery time, showing better long-term stability, compared with the sensor based on the CeO_2 nanoparticles. The long-term stability may be explained by the chemical states at the surface, thus, UPS was employed, as shown in the Fig. 33(c), in which Si 2*p* core-level spectra were measured after the samples were exposed to the HMDSO gas for 24 h with sputtering time to determine if SiO_2 was created at the surface. In Pd decorated nanowires, the main peak at 103.6 eV was observed, assigned to the Si-O bond, originated from the SiO_2 layer. The peak intensity decreased with the sputtering time, meaning that the SiO_2 layer was thicker at the surface of the nanowires. When CeO_2 nanoparticles and CeO_2 nanoparticles/rGO layer were coated onto the nanowires, there was no significant change in the peak intensity. However, when the CeO_2 nanoparticles/rGO layer was peeled off, the peak intensity significantly decreased. This means that the HMDSO was not reached at the nanowires through the layer, thereby, the SiO_2 layer formed at the nanowires was thin. This may explain the enhancement of the stability of the sensors.

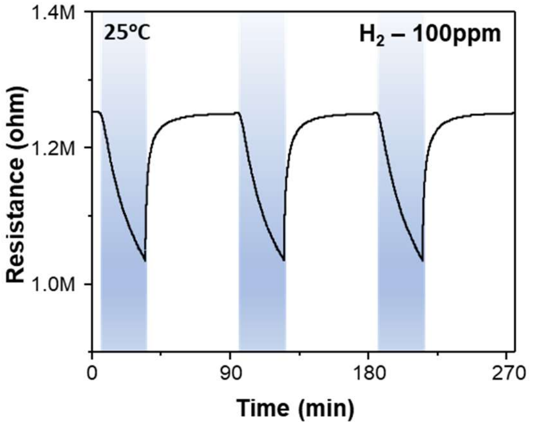

Figure 34. The resistance change of CeO_2/rGO/Pd/ZnO nanowires toward H_2 of 100 ppm measured at 25°C.

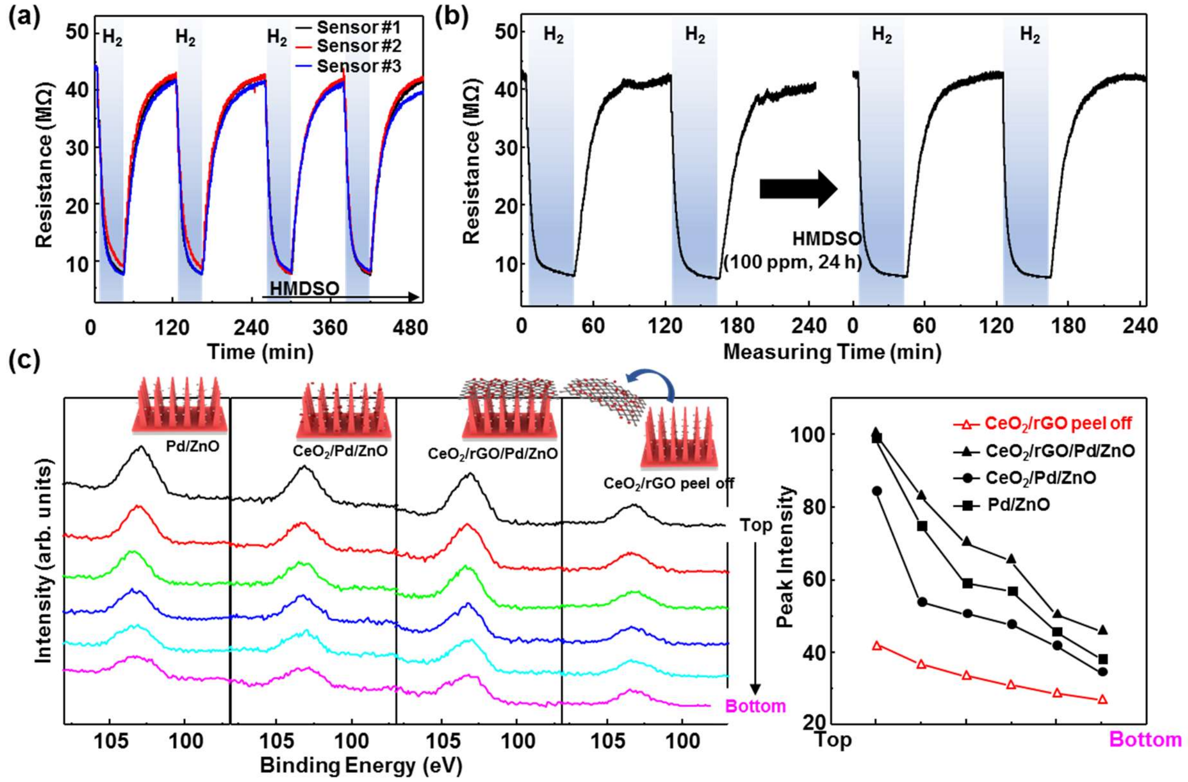

Figure 35. (a) The responses of the CeO_2/rGO-decorated Pd-ZnO nanowires sensor toward H_2 (100 ppm) gas under air and air/HMDSO (100 ppm)), measured at 250°C. 3 sensors were fabricated, tested. (b) The responses of CeO_2/rGO-coated Pd-ZnO nanowires sensor toward H_2 (100 ppm) gas before and after the HMDSO exposure for 24 h. (c) Si 2*p* core level spectra of Pd-ZnO, CeO_2-decorated Pd-ZnO, CeO_2/rGO-coated Pd-ZnO nanowires with sputtering time to see the chemical states from the top to the bottom side of the nanowires after all samples are exposed to HMDSO gas for 24 h. The change of the peak intensity is also summarized.

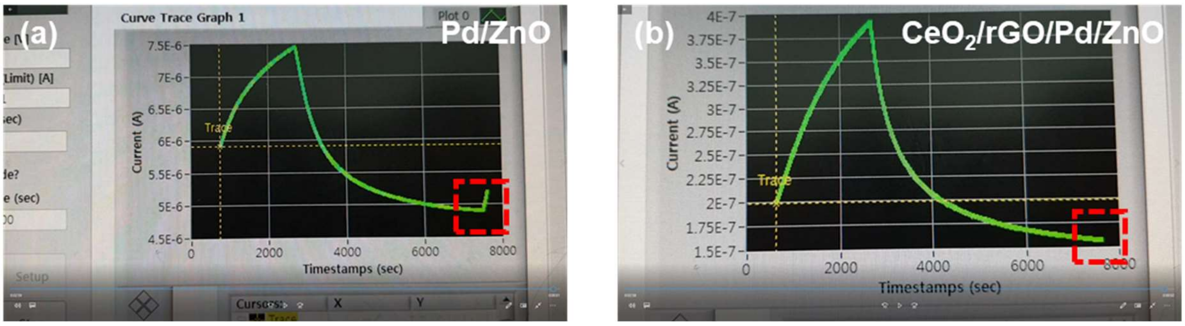

Figure 36. The captured images showing the gas response and HMDSO exposure reaction of fabricated sensor device.

For further investigation of the gas-sensing performances, the sensing curves of the CeO$_2$/rGO/Pd/ZnO samples were recorded with H$_2$ concentrations ranging from 40 ppm to 100 ppm at 250°C, as shown in Fig. 35(a). It is clearly seen that the response increased with H$_2$ concentrations and the limit of detection (LOD) was found to be approximately 0.46 ppm, determined by extrapolating the sensing curves in the inset. The response was also measured as a function of temperature from 25°C to 250°C, plotted in Fig. 35(b). At low temperatures less than 50°C, there was no significant response with the H$_2$. As the temperature increased, the response also increased and reached to 5.45 at 250°C. By comparing the change of the responses with the gas concentration and the temperature (Fig. 36(a)), it was concluded that 1°C temperature change had the same effect on the sensor signal with 1.75 (ppm) target gas concentration change. Finally, the sensor was exposed to various gases such as H$_2$, NO$_2$, SO$_2$, and CO at a concentration of 0.8 ppm to investigate the selective gas detection, as plotted in Fig. 36(b). Among the gases, the response of the sensor toward NO$_2$ was higher than the responses toward other gases, as summarized in Fig. 36(c). However, it seems that the sensor senses all the gases. This may be explained via the similar sensing mechanisms of the Pd-ZnO nanowires toward all gases, that is, the spill-over effects of the gas molecules on the surface of the oxide or the Pd enabling them to react with the adsorbed oxygen species.[50-52] The Pd also increases the number of the chemisorbed oxygen species, increasing the sensitivity of all gases.

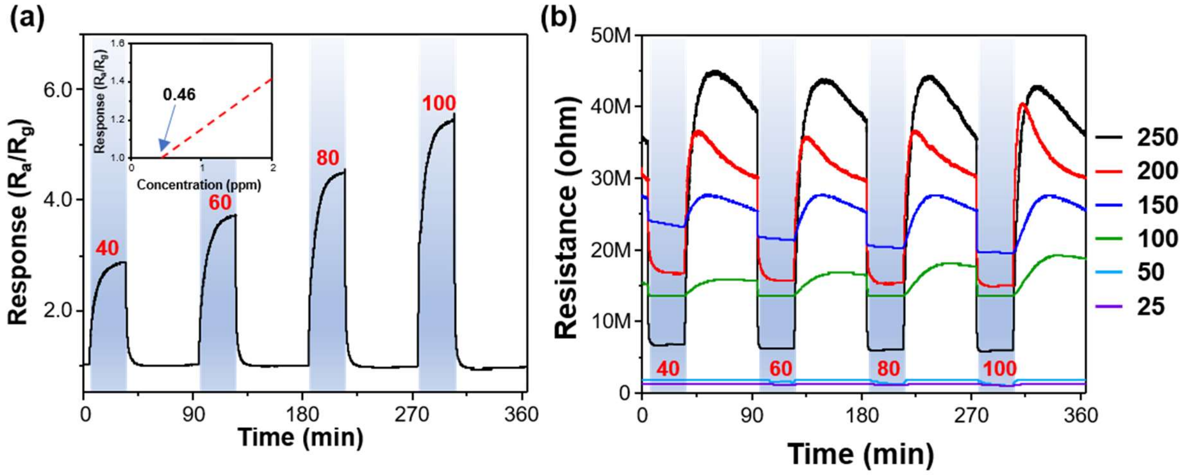

Figure 37. (a) Response of CeO_2/rGO/Pd/ZnO sensor as a function of H_2 concentration and (b) Resistance change with temperature.

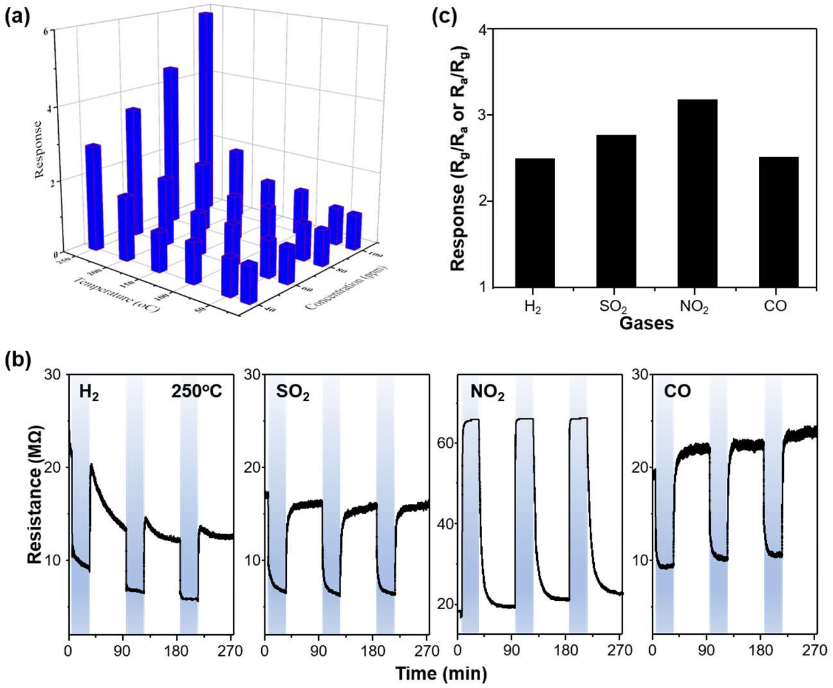

Figure 38. (a) 3 dimensional plot of the responses with temperature and H_2 concentration. (b) Resistance change in CeO_2/rGO/Pd/ZnO sensor toward H_2, SO_2, CO, and NO_2 gases at 250°C (c) Summary of responses toward H_2, SO_2, CO, and NO_2 gases

4.4 Conclusion

In summary, we demonstrated that the Pd nanoparticles-decorated ZnO nanowires sensor had quite a reliable hydrogen sensing performance by introducing the CeO_2 nanoparticles and the rGO layer in an HMDSO (100 ppm) environment. The CeO_2/rGO mixture was synthesized via a simple impregnation method, in which the rGO was found to be quite porous and covering the surface of the nanowires. The HMDSO reaction at the surface of the nanowires decreased the hydroxyl groups and increased the oxygen vacancies, resulting in a decrease of the response and baseline resistance. The CeO_2 supplied sufficient oxygen to the surface of the nanowires, keeping the surface-chemical process less sensitive to the HMDSO. However, the CeO_2-decorated sensors showed that the gas response degraded as the HMDSO exposure time increased to 24 h. UPS measurement showed that it might be due to an increase in the thickness of the SiO_2 layer, which was remarkably decreased by introducing an rGO layer acting as a filter for the HMDSO. Thus, the sensor designs displayed excellent long-term stability to HMDSO exposure.

4.5 References

[1] J. Guo, J. Zhang, H. Gong, D. Ju, B. Cao, Au nanoparticle-functionalized 3D SnO_2 microstructures for high-performance gas sensor, Sens. Actuators B: Chem 226 (2016) 266-272.

[2] C.M. Ghimbeu, M. Lumbreras, M. Siadat, R.C. van Landschoot, J. Schoonman, Electrostatic sprayed SnO_2 and Cu-doped SnO_2 films for H_2S detection, Sens. Actuators B: Chem 133 (2008) 694-698.

[3] S. Öztürk, A. Kösemen, Z.A. Kösemen, N. Kılınç, Z.Z. Öztürk, M. Penza, Electrochemically growth of Pd doped ZnO nanorods on QCM for room temperature VOC sensors, Sens. Actuators B: Chem 222 (2016) 280-289.

[4] Y. Wang, F. Qu, J. Liu, Y. Wang, J. Zhou, S. Ruan, Enhanced H_2S sensing characteristics of CuO-NiO core-shell microspheres sensors, Sens. Actuators B: Chem 209 (2015) 515-523.

[5] Y.V. Kaneti, J. Yue, J. Moriceau, C. Chen, M. Liu, Y. Yuan, X. Jiang, A. Yu, Experimental and theoretical studies on noble metal decorated tin oxide flower-like nanorods with high ethanol sensing performance, Sens. Actuators B: Chem 219 (2015) 83-93.

[6] J. Wang, P. Yang, X. Wei, High-performance, room-temperature, and no-humidity-impact ammonia sensor based on heterogeneous nickel oxide and zinc oxide nanocrystals, ACS Appl. Mater. Interfaces 7 (2015) 3816-3824.

[7] H.-R. Kim, A. Haensch, I.-D. Kim, N. Barsan, U. Weimar, J.-H. Lee, The role of NiO Doping in reducing the impact of humidity on the performance of SnO_2-based gas sensors: synthesis strategies, and phenomenological and spectroscopic studies, Adv. Funct. Mater. 21 (2011) 4456-4463.

[8] K.-R. Park, H.-B. Cho, J. Lee, Y. Song, W.-B. Kim, Y.-H. Choa, Design of highly porous SnO2-CuO nanotubes for enhancing H_2S gas sensor performance, Sens. Actuators B: Chem 302 (2020) 127179.

[9] J. M. Baik, M. H. Kim, C. Larson, C. T. Yavuz, G. D. Stucky, A. M. Wodtke, M. Moskvits, Pd-Sensitized Single Vanadium Oxide Nanowires Highly Responsive Hydrogen Sensing Based on the Metal-InsulatorTransition, Nano Lett. 9 (2009) 3980-3984.

[10] J. M. Baik, M. Zielke, M. H. Kim, K. L. Turner, A. M. Wodtke, M. Moskovits, Tin-oxide-nanowire-based electronic nose using heterogeneous catalysis as a functionalization strategy, ACS Nano 4 (2010) 3117-3122.

[11] K.K. Sharma, R.B. Patel, H. Singh, A Reliable and Energy Efficient Transport Protocol for Wireless Sensor Networks, International journal of Computer Networks & Communications, 2 (2010) 92-

103.

[12] A. Mesmoudi, M. Feham, N. Labraoui, Wireless Sensor Networks Localization Algorithms: A Comprehensive Survey, International journal of Computer Networks & Communications, 5 (2013) 45-64.

[13] R. Piyare, S.R. Lee, Towards Internet of Things (IOTS): Integration of Wireless Sensor Network to Cloud Services for Data Collection and Sharing, International journal of Computer Networks & Communications, 5 (2013) 59-72.

[14] M. Aleixandre, M. Gerboles, Review of small commercial sensors for indicative monitoring of ambient gas, Chem. Eng. Trans. 30 (2012) 169-174.

[15] V. Palmisano, E. Weidner, L. Boon-Brett, C. Bonato, F. Harskamp, P. Moretto, M.B. Post, R. Burgess, C. Rivkin, W.J. Buttner, Selectivity and resistance to poisons of commercial hydrogen sensors, Int. J. Hydrog. Energy 40 (2015) 11740-11747.

[16] G.F. Fine, L.M. Cavanagh, A. Afonja, R. Binions, Metal oxide semi-conductor gas sensors in environmental monitoring, Sensors 10 (2010) 5469-5502.

[17] C.H. Kwak, T.H. Kim, S.Y. Jeong, J.W. Yoon, J.S. Kim, J.H. Lee, Humidity-Independent Oxide Semiconductor Chemiresistors Using Terbium-Doped SnO2 Yolk-Shell Spheres for Real-Time Breath Analysis, ACS Appl Mater Interfaces, 10 (2018) 18886-18894.

[18] X.-H. Ma, H.-Y. Li, S.-H. Kweon, S.-Y. Jeong, J.-H. Lee, S. Nahm, Highly Sensitive and Selective PbTiO3 Gas Sensors with Negligible Humidity Interference in Ambient Atmosphere, ACS Appl. Mater. Interfaces 11 (2019) 5240-5246.

[19] M. Nishibori, K. Katoh, T. Itoh, N. Izu, W. Shin, Deactivation mechanism of alumina supported Pt and Pd catalysts for gas sensor by hexamethyldisiloxane (HMDSO), IMCS (2012) 1745-1747.

[20] J. J. Ehrhardt, L. Colin, D. Jamois, Poisoning of platinum surfaces by hexamethlydisiloxane (HMDS): application to catalytic methane sensors, Sens. Actuators B: Chem 40 (1997) 117-124.

[21] M. Matsumiya, W. Shin, F. Qiu, N. Izu, I. Matsubara, N. Murayama, Poisoning of platinum thin film catalyst by hexamethyldisiloxane (HMDS) for thermoelectric hydrogen gas sensor, Sens. Actuators B: Chem 96 (2003) 516-522.

[22] K. Arnby, M. Rahmani, M. Sanati, N. Cruise, A.A. Carlsson, M. Skoglundh, Characterization of Pt/γ-Al_2O_3 catalysts deactivated by hexamethyldisiloxane, Appl. Catal. B-Environ. 54 (2004) 1-7.

[23] M. Schüler, T. Sauerwald, A. Schütze, A novel approach for detecting HMDSO poisoning of metal oxide gas sensors and improving their stability by temperature cycled operation, Journal of Sensors

and Sensor Systems, 4 (2015) 305-311.

[24] G. Tournier, C. Pijolat, Selective filter for SnO-based gas sensor: application to hydrogen trace detection, Sens. Actuators B: Chem, 106 (2005) 553-562.

[25] J. E. Chilton, J. N. Baran, W. E. Thomas, L. J. E. Hofer, J. L. Snyder, SILICONE VAPOR POISOINING OF CATALYTIC METHANE SENSORS, Proceedings of the Fourth WVU Conference on Coal Mine Electrotechnology (1978)

[26] J.X. Wang, X.W. Sun, Y. Yang, H. Huang, Y.C. Lee, O.K. Tan, L. Vayssieres, Hydrothermally grown oriented ZnO nanorod arrays for gas sensing applications, Nanotechnology 17 (2006) 4995-4998.

[27] B. Ye, B. Jeong, M. Lee, H.-D. Kim, J.M. Baik, Low-Temperature De-NO_x Extruded monolithic catalysts based on highly dispersive Mn-Ce oxide nanoparticles of low Ce content, Adv. Mater. Technol. 4 (2019) 1800462-1800468.

[28] B. Ye, M. Lee, B. Jeong, J. Kim, D.H. Lee, J.M. Baik, H.-D. Kim, Partially reduced graphene oxide as a support of Mn-Ce/TiO_2 catalyst for selective catalytic reduction of NO_x with NH_3, Catalysis Today 328 (2019) 300-306.

[29] R. Verma, S.K. Samdarshi, In situ decorated optimized CeO_2 on reduced graphene oxide with enhanced adsorptivity and visible light photocatalytic stability and reusability, J. Phys. Chem. C 120 (2016) 22281-22290.

[30] S.D. Perera, R.G. Mariano, K. Vu, N. Nour, O. Seitz, Y. Chabal, K.J. Balkus, Hydrothermal synthesis of graphene-TiO_2 nanotube composites with enhanced photocatalytic activity, ACS Catalysis 2 (2012) 949-956.

[31] R. Ma, M. Jahurul Islam, D. Amaranatha Reddy, T.K. Kim, Transformation of CeO2 into a mixed phase CeO_2/Ce_2O_3 nanohybrid by liquid phase pulsed laser ablation for enhanced photocatalytic activity through Z-scheme pattern, Ceramics International 42 (2016) 18495-18502.

[32] Z. Wang, P. Zhao, D. He, Y. Cheng, L. Liao, S. Li, Y. Luo, Z. Peng, P. Li, Cerium oxide immobilized reduced graphene oxide hybrids with excellent microwave absorbing performance, Phys. Chem. Chem. Phys. 20 (2018) 14155-14165.

[33] . Sagadevan, M.R. Johan, J.A. Lett, Fabrication of reduced graphene oxide/CeO_2 nanocomposite for enhanced electrochemical performance, Appl. Phys. A 125 (2019).

[34] L. Xu, W.Q. Huang, L.L. Wang, G.F. Huang, Interfacial interactions of semiconductor with graphene and reduced graphene oxide: CeO_2 as a case study, ACS Appl. Mater. Interfaces 6 (2014)

20350-20357.

[35] Q. Hao, G. Cui, Y. Tian, T. Tan, Y. Zhang, Three-dimensional S/CeO_2/RGO composites as cathode materials for lithium(-)sulfur batteries, Materials 11 (2018).

[36] S. Wang, F. Gao, Y. Zhao, N. Liu, T. Tan, X. Wang, Two-dimensional CeO_2/RGO composite-modified separator for lithium/sulfur batteries, Nanoscale Res. Lett. 13 (2018) 377.

[37] D. Martin, D. Duprez, Mobility of surface species on oxides. 1. Isotopic Exchange of $^{18}O_2$ with ^{16}O of SiO_2, Al_2O_3, ZrO_2, MgO, CeO_2, and CeO_2-Al_2O_3. Activation by Noble Metals. Correlation with Oxide Basicity, J. Phys. Chem. 100 (1996) 9429-9438..

[38] Z. Wu, M. Li, J. Howe, H.M. Meyer, 3rd, S.H. Overbury, Probing defect sites on CeO_2 nanocrystals with well-defined surface planes by Raman spectroscopy and O_2 adsorption, Langmuir 26 (2010) 16595-16606.

[39] J.W. Yoon, J.S. Kim, T.H. Kim, Y.J. Hong, Y.C. Kang, J.H. Lee, A New strategy for humidity independent oxide chemiresistors: dynamic self-refreshing of In_2O_3 sensing surface assisted by layer-by-layer coated CeO_2 nanoclusters, Small 12 (2016) 4229-4240.

[40] C. Zhang, J. Zhang, Y. Su, M. Xu, Z. Yang, Y. Zhang, ZnO nanowire/reduced graphene oxide nanocomposites for significantly enhanced photocatalytic degradation of Rhodamine 6G, Physica E: Low-dimensional Systems and Nanostructures 56 (2014) 251-255.

[41] C.W. Na, J.-H. Kim, H.-J. Kim, H.-S. Woo, A. Gupta, H.-K. Kim, J.-H. Lee, Highly selective and sensitive detection of NO_2 using rGO-In_2O_3 structure on flexible substrate at low temperature, Sens. Actuators B: Chem. 255 (2018) 1671-1679.

[42] S. C. Tsang, C. D. A. Bulpitt, P. C. H. Mitchell, A. J. R- Cuesta, Some New Insights into the Sensing Mechanism of Palladium Promoted Tin (IV) OxideSensor, J. Phys. Chem, B 105 (2001) 5737-5742.

[43] I. Kocemba, J. Rynkowski, The influence of catalytic activity on the response of Pt/SnO_2 gas sensors to carbon monoxide and hydrogen, Sens. Actuators B: Chem 155 (2011) 659-666.

[44] J. Bang, K. J. Chang, Atomic Structure and Diffusion of Hydrogen in ZnO, J. Kor. Phys. Soc. 55 (2009) 98-102.

[45] R.H. Doremus, Diffusion of water in silica glass, J. Mater. Research 10 (2011) 2379-2389.

[46] N.E. Blanchard, V.V. Naik, T. Geue, O. Kahle, D. Hegemann, M. Heuberger, Response of Plasma-Polymerized Hexamethyldisiloxane Films to Aqueous Environments, Langmuir, 31 (2015) 12944-12953.

[47] H.Y. Li, C.S. Lee, D.H. Kim, J.H. Lee, Flexible Room-Temperature NH_3 Sensor for Ultrasensitive, Selective, and Humidity-Independent Gas Detection, ACS Appl. Mater. Interfaces 10 (2018) 27858-27867.

[48] A. Helwig, A. Hackner, G. Muller, D. Zappa, G. Sberveglieri, Self-Test Procedures for Gas Sensors Embedded in Microreactor Systems, Sensors, 18 (2018)

[49] M. Schuler, T. Fricke, T. Sauerwald, A. Schutze, Detecting poisoning of metal oxide gas sensors at an early stage by temperature cycled operation, AMA conferences (2015) 735-739.

[50] C. M. Chang, M. H. Hon, I. C. Leu, Imprlcspplovement in CO sensing characteristics by decorating ZnO nanorod arrays with Pd nanoparticles and the related mechanisms, RSC Advances, 2012, 2, 2469–2475

[51] P. Rai, Y. S. Kim, H. M. Song, M. K. Song, Y. T. Yu, The role of gold catalyst on the sensing behavior of ZnO nanorods for CO and NO_2 gases, Sens. Actuators B: Chem 165 (2012) 133-142.

[52] C. M. Chang, M. H. Hon, I. C. Leu, Outstanding H_2 Sensing Performance of Pd Nanoparticle-Decorated ZnO Nanorod Arrays and the Temperature-Dependent Sensing Mechanisms, ACS Appl. Mater. Interfaces 5 (2013) 135-143.

CURRICULUM VITAE

Yeong Min Kwon

Street Address: UNIST-gil 50, Eonyang-eup, Ulju-gun, Ulsan, Republic of Korea, 44919.
E-mail: kwonym@unist.ac.kr / kwonym4023@gmail.com · Phone: +82-10-6495-4023

EDUCATION

2016-2021 **Ulsan National Institute of Science and Technology (UNIST)**

- Ph.D in Materials Science and Engineering.
- Supervisor: Professor, Kyoung-Jin Choi
- Supervisor: Professor, Jeong Min Baik

2010-2016 **Pukyong National University (PKNU)**

- B.S. in Materials Science and Engineering

TEACHING EXPERIENCE

Teaching Assistant

2018, Spring **Teaching Assistant, Materials Lab1,** Department of Materials Science and Engineering, Ulsan National Institute of Science and Technology

2018, Fall **Teaching Assistant, Introduction to Semiconductor,** Department of Materials Science and Engineering, Ulsan National Institute of Science and Technology

---

HONORS

2020

- **Minister`s Award**
  Ministry of Trade, Industry & Energy
- **Best Poster Award**
  2020 Spring Meeting of The Korean Ceramic Society

PUBLICATION

1. Subin Choi, Chan Sam Park, Hee Young Chae, Byungjoo Oh, Jongmin Lee, **Yeong Min Kwon**, Jeong Min Baik, Heungjoo Shin, Jae Joon Kim*, "A Wide Dynamic Range Multi-Sensor ROIC for Portable Environmental Monitoring Systems With Two-Step Self-Optimization Schemes", IEEE Transactions on Circuits and Systems I: Regular Papers, doi: 10.1109/TCSI.2021.3065503 (2021).

2. **Yeong Min Kwon,** Hee-Jun Kim, Bora Ye, Hong-Dae Kim, Yun Sik Lee,

Heungjoo Shin, Jeong Min Baik*, “Ce oxide nanoparticles on porous reduced graphene oxides for stable hydrogen detection in air/HMDSO environment”, **Sensors and Actuators B: Chemical**, Vol. 321, p. 128529 **(2020)**.

3. Rahul Purbia, **Yeong Min Kwon**, Hong-Dae Kim, Yun Sik Lee, Heungjoo Shin, Jeong Min Baik*, “Zero-dimensional heterostructures: N-doped graphene dots/SnO$_2$ for ultrasensitive and selective NO$_2$ gas sensing at low temperatures”, **J. Mater. Chem. A,** Vol. 8, p. 11734-11742 **(2020)**.

4. **Yeong Min Kwon**, Yeongjin Lim, Hye Jin Lee, Yun Sik Lee, Heungjoo Shin, Jeong Min Baik*, “Electron Exchange Process Control Between Silver Nanoparticles and Metal-Oxides for Highly Selective Gas Detection”, **2018 IEEE SENSORS**, p. 1-5 **(2018)**.

5. Amit Sanger, Sung Bum Kang, Myeong Hoon Jeong, Min Ji Im, In Young Choi, Chan Ul Kim, Hyungmin Lee, **Yeong Min Kwon**, Jeong Min Baik, Ho Won Jang, Kyoung Jin Choi*, “Morphology-Controlled Aluminum-Doped Zinc Oxide Nanofibers for Highly Sensitive NO$_2$ Sensors with Full Recovery at Room Temperature”, **Adv. Sci.**, Vol. 5, pp. 1800816 **(2018)**.

6. Yeongjin Lim, Soosung Kim, **Yeong Min Kwon**, Jeong Min Baik, Heungjoo Shin*, “A highly sensitive gas-sensing platform based on a metal-oxide nanowire forest grown on a suspended carbon nanowire fabricated at a wafer level”, Sensors and Actuators B 260 (2018) 55–62, Vol. 260, pp. 55-62 **(2018)**.

7. Yeongjin Lim, Seungwook Lee, **Yeong Min Kwon**, Jeong Min Baik, Heungjoo Shin*, “Gas sensor based on a metal oxide nanowire forest built on a suspended carbon nano-heater”, 2018 IEEE Micro Electro Mechanical Systems (MEMS) **(2018)**.

8. Seungkyu Kim, Yejong Yu, Sang Yun Jeong, Mi Gyoung Lee, Hye Won Jeong, **Yeong Min Kwon**, Jeong Min Baik, Hyunwoong Park, Ho Won Jang, Sanghan Lee*, “Plasmonic gold nanoparticle-decorated BiVO 4/ZnO nanowire heterostructure photoanodes for efficient water oxidation”, **Catal. Sci. Technol.**, Vol. 8, pp. 3759-3766 **(2018)**.

PATENTS

1. Jeong Min Baik, **Yeong Min Kwon**, “Gas sensor and manufacturing method thereof.” Korea, Patent No. 10-2019-0175907 (2019).

2. **[Patent Registration]** Jeong Min Baik, **Yeong Min Kwon,** Kyeong Nam Kim, “Hydrogen gas sensor” Korea, Patent No. 10-2017-0070967 (2017), 1019532950000 (2019).

3. **[Patent Registration]** Jeong Min Baik, **Yeong Min Kwon**, Kyeong Nam Kim, "Gas sensor and manufacturing method thereof" Korea, Patent No. 10-2017-0068662 (2017), 1019687310000 (2019).

4. **[Patent Registration]** Jeong Min Baik, Heungjoo Shin, **Yeong Min Kwon**, Yeongjin Lim, Junyeong Seo, "HYBRID NANO-WIRE GROWING METHOD." Korea, Patent No. 10-2016-0078664 (2016), 10-19105350000 (2018).

PRESENTATION

1. 2020 Fall conference of The Korean Sensors Society, Korea, November 11-13, 2020. **Poster:** Low Temperature Electrochemical sensor for Pentane Gas Detection.

2. 2020 Spring Meeting of The Korean Ceramic Society, Korea, July 6 – 9, 2020. **Poster:** Highly dispersive Ceria nanoparticles on porous reduced graphene oxide for highly stable hydrogen detection in air/HMDSO environment.

3. The 26th Korean Conference on Semiconductors, Korea, February 13 – 15, 2019. **Oral:** Wafer-scale grown multiple metal oxide nanowires for gas sensor.

4. 2018 Fall conference of the Korean institute of metals and materials, Korea, October 24 –26, 2018. **Poster:** Electron exchange process control between silver nanoparticles and metal-oxides for highly selective gas detection.

5. SENSORS 2018 : The 17th IEEE Conference on Sensors (IEEE Sensors 2018), India, October 28 – 31, 2018. **Poster:** Electron exchange process control between silver nanoparticles and metal oxides for highly selective gas detection.

6. Nano Korea 2018, Korea, July 10 – 13, 2018. **Poster :** A highly selective sensor based on multiple silver-and palladium-decorated nanowires grown hydrothermally at a wafer level.

7. 7th GOSPEL, Korea, November 8 – 10, 2017. **Poster:** Hybrid metal oxide nanowire semiconductor for gas sensor..

8. International Conference on Electronic Materials and Nanotechnology for Green Environment (ENGE 2016), Korea, November 6 – 9, 2016. **Poster:** Hybrid Metal Oxide Nanowire Semiconductor for Gas Sensor.

SKILLS

Technical: Gas sensor testing, Growth of metal oxide nanowire, Synthesis of metal oxide nanoparticles, Synthesis of yolk-shell structure, Photolithography

Laboratory Material analysis (SEM, XRD, UPS), Processing equipment (E-beam evaporator, Sputter, Doctor blade, Centrifugation, Langmuir Blodgett, Photo mask Aligner), Measurement equipment (Probe station, source meter, Electrometer, pH meter, Potentiostat), PL

Computer: Origin Lab, Rhinoceros, Microsoft office